Delft University of Technology

Thesis

The impact of high resolution surface reflectance data on the accuracy of the TROPOMI tropospheric NO_2 product over the greater Rotterdam region

Niek Bossers 4153626

February 14, 2019

Thesis committee:
Dr. T. Vlemmix (daily supervisor)
Prof.dr. P.F. Levelt
Dr. J.P. Veefkind
Dr.ir. A.A. Verhagen

Abstract

The Sentinel-5 Precursor satellite has a payload of the TROPOspheric Monitoring Instrument, TROPOMI. The satellite was launched in 2017 by ESA with the intended goal of measuring trace gases in the atmosphere (NO_2, O_3, SO_2, $HCHO$, CO, CH_4). Its predecessor, called Ozone Monitoring Instrument, OMI, has been launched in 2004 and has produced atmospheric composition measurements since then. TROPOMI will continue this data-series.

One of the products of TROPOMI is the *Tropospheric NO_2 column*. This product is based on the spectral measurements to obtain the column abundance of NO_2 in the troposphere. This product also relies on a-priori data and one of the most important of these a-priori datasets is the albedo dataset. The currently used dataset has a resolution of 0.5°x 0.5°, which corresponds to approximately 55 km x 34 km at mid-latitudes. This dataset is called the OMI LER albedo climatology, which is a global monthly albedo dataset based on the satellite measurements made by the *Ozone Monitoring Instrument* (OMI). The TROPOMI pixel size is significantly smaller, 3.5 km x 7 km. Due to this large difference in resolution the discussion arises if this used dataset is sufficient for accurate results. This research makes a comparison between the current a-priori dataset and possible replacements, which have a higher resolution.

This paper makes this comparison by calculating *Air Mass Factors* (AMFs) using the OMI LER albedo climatology as a reference and the two alternative high resolution surface reflectance datasets, Sentinel-2 and Landsat-8. These surface reflectance datasets were regridded and averaged on the corresponding TROPOMI grid. The focus area of this paper is the *Greater Rotterdam* region in the Netherlands.

Before these AMF calculations were done, a comparison between Sentinel-2 and Landsat-8 surface reflectance datasets is made. This is done both on their own high resolution and regridded onto the TROPOMI grid. This comparison showed that the Sentinel-2 dataset consisted of two tiles which were processed independently, leading to an inconsistency roughly in the middle of the focus area. It also became apparent that above water surfaces and land covered by vegetation a bias of approximately 0.01 was present between the two high resolution surface reflectance datasets. These differences are relatively small. The differences calculated for the datasets regridded to the TROPOMI grid were also relatively small, with a bias of 0.01 above the water and vegetation surfaces.

Two cases were studied during this research: the 21st of April 2018 and the 6th/7th of May 2018. These days were selected because of cloud free conditions and overpasses of all the needed satellites. The results show that significant improvements can be made by using a higher resolution surface reflectance dataset. A median bias of -10.4% (-15.6%) was calculated for the 21st of April for Sentinel-2 (Landsat-8) compared to the AMFs based on the OMI albedo dataset. For May this was -3.9% (-9.3%). Furthermore this study showed extreme AMF-biases of 68.0% overestimation and 39.8% underestimation by the OMI albedo dataset compared to Sentinel-2, where the overestimation was observed over the greenhouses in the Westland region and the underestimation in the rural region to the East of the domain in April. For May the underestimation was mostly observed to the West (North Sea), indicating that over regions with a low surface reflectance the atmospheric correction greatly influences the AMF. The comparison between Landsat-8 and OMI showed similar results in the AMF differences.

These findings are supported further by a recent Sentinel-5P validation study, which compared ground based observations to the TROPOMI observations. This project found an NO_2 underestimation of approximately 20% for many different stations. This research suggest that, at least partly, this difference can be explained by the coarse resolution of the a-priori albedo dataset used. Future development of a high resolution SR climatology is essential for a more accurate TROPOMI NO_2 product.

Contents

1 Introduction

Since 2004 the *Ozone Monitoring Instrument* (OMI) has been making global coverage atmospheric composition measurements globally. This atmospheric composition measuring is done by making observations of the atmospheric constituents, which consist of trace gases, aerosols and clouds. The atmospheric constituents have an effect on the ultraviolet and/or the visible part of the electromagnetic spectrum. OMI therefore makes measurements in these parts of the spectrum. OMI is aboard the NASA spacecraft *Aura*, with an orbit time of 100 minutes. This instrument has provided crucial atmospheric data, regarding the content of: $O_3, NO_2, SO_2, HCHO$ and aerosol concentrations, and time-series which has been used by numerous agencies and governments. OMI was built to last approximately 5 years [1] but is has already been operational for 14 years. Due to this large overextension of its operational life, the instrument is reaching its limits regarding its capabilities of remaining operational. Part of this is due to radiation damage on the sensors. This damage leads to loss of measurement quality [2].

In 2017 the *European Space agency* (ESA) launched the *Tropospheric Monitoring Instrument* (TROPOMI) on board the Sentinel-5 Precursor satellite. This instrument was designed with the goal of replacing OMI and also to continue the time-series started by OMI, and its predecessors: GOME, GOME-2 and SCIAMACHY [3]. This instrument was built with an intended lifespan of 7 years but it is hoped that, like OMI, its actual lifespan will be considerably longer [1].

Both OMI and TROPOMI are passive instruments, which means that both of them rely on the reflection of sunlight for making their measurements. Both OMI and TROPOMI sense the reflected solar radiation in the visible part of the electromagnetic spectrum and in the ultraviolet part. TROPOMI also makes measurements in the longer wavelength part of the spectrum, the shortwave infrared.

NO_2 is one of the main gases measured by both instruments. NO_2 and NO together are called NO_x. NO_x are gaseous compounds created during the combustion of fossil fuels, so sources include: power plants, traffic, industry, shipping. Natural sources also occur, and the gas can also be created in lightning events. In urban areas the sources are mainly in internal combustion engines. NO_x is therefore one of the more characteristic air pollutants created by traffic.

NO_x measurements are very important since NO_x, and mainly NO_2, causes both health and environmental problems. The health problems consist mainly of respiratory problems, for example the development of asthma in case of long-term exposure. The issue with NO_2 is that its emissions are often in the proximity of people, for example a busy road in a city, or a highway close to where people live [4]. The environmental effects cover a wide spectrum of problems. NO_x in the atmosphere contributes to nutrient pollution in coastal waters, by nitrate aerosols forming using this NO_x [5]. NO_x can also cause haziness, so less visibility and another big problem is that NO_2 and NO_x can cause acid rain, which is harmful for the environment [6]. By having access to accurate data and also time-series of the data in the form of NO_2 maps, governments and agencies are able to develop policies for the reduction of NO_x emissions and also to check if implemented measures are working and giving the desirable effects. It is also possible to check whether different companies and other institutions are following the rules set by the government.

The amount of information that satellites can provide in order to facilitate users, depends on factors such as the precision, accuracy and resolution of the data. Resolution encompasses different types. The first type is called *spatial resolution*. This is the size of the pixel that the instrument produces. The second type, *spectral resolution*, is a measure of the ability of the instrument to discriminate spectral lines. The third type of resolution, temporal resolution, can be seen as the time between two different observations [7].

When these types of resolution are applied to OMI and TROPOMI it can be seen that the biggest resolution difference is the difference in spatial resolution. OMI has a resolution ranging from 13 km x 24 km at nadir to 13 km x 100 km at the side of the swath, while TROPOMI has a spatial resolution of 7 km x 3.5 km, which is also more constant across the swath. This is a major difference in resolution and it is one of the big advantages of the newer TROPOMI data. Another big advantage is that TROPOMI does not only have a higher resolution, but also a better signal-to-noise ratio [8].

The accuracy of the satellite products depends in various ways on the accuracy of the input data, so called a-priori data, which is needed in order to solve the ill-posed retrieval problem. The retrieval is ill-posed due to the spectral measurements themselves not containing all the needed information necessary

to infer tropospheric columns or profiles. In the case of TROPOMI the most criticised and uncertain a-priori data are mainly the surface albedo and the trace gas and aerosol extinction profiles.

The surface albedo input data used for the TROPOMI product is based on the surface albedo dataset acquired by the OMI mission over the years. It has a resolution of 0.5°x 0.5°, which is not the same as OMI's resolution itself. This surface albedo database, with a significantly lower spatial resolution than the TROPOMI data, works when it is applied to large areas. However, since the resolution of the TROPOMI dataset is higher than the resolution of the OMI dataset, it is to be expected that a more accurate dataset for the surface albedo will improve the product, especially when applied to city-scale observations. Surface reflectance datasets with a significantly higher resolution than the OMI surface albedo product are available. Two examples of these higher resolution surface reflectance datasets are the ones produced by NASA's *Landsat-8* satellite and ESA's *Sentinel-2* satellite. Both satellites have produced products with a spatial resolution of tens of metres, for individual overpasses, in comparison with OMI's resolution of tens of kilometres, which is a monthly product.

1.1 Research objectives & Methodology

This thesis addresses the following research questions:

- What is the accuracy of the Sentinel-2 surface reflectance product at its native resolution and on the spatial resolution of TROPOMI?
- What is the impact on the acurracy of the TROPOMI tropospheric NO_2 product of alternative prior surface reflectance information from Sentinel-2?

The accuracy and precision of the high resolution surface reflectance products, Sentinel-2 and Landsat-8, can be investigated by mutual comparison as the two instruments have a similar spatial resolution, overpass time and spectral channel in the spectral region relevant for NO_2 (see chapter 3). In this research the Sentinel-2 data will be used as baseline, while Landsat-8 is used for verification.

In order to investigate the impact of alternative surface reflectance information, a regional case-study with a limited amount of data has been chosen. The area chosen is the *Greater Rotterdam Area* in the West of the Netherlands, as can be seen in figure 1.1.

Figure 1.1: The Greater Rotterdam area, the focus area of this research.

This area was chosen due to the fact that this area is densely populated, the city of Rotterdam alone is the second biggest city in the Netherlands and this does not include all the cities close to Rotterdam. Apart form being densely populated the area is also very heavily industrialised, with industry being one of the bigger parts of the local economy. The harbour of Rotterdam is also very interesting for this research. This harbour used to be the biggest in the world, and it is still the biggest harbour of Europe today. This harbour and its transportation, together with the high population number, which causes high traffic flows, and the industry lead to high air pollution. Satellite data can help to distinguish sources and source categories such that effective local policies can be developed in order to reduce people's exposure to air pollution.

The Rijnmond area also covers different types of landcover, which can have quite different surface reflectance values. The Rijnmond area's most distinguishable land covers are: Urban (mainly Rotterdam), rural (*Hoeksche Waard*), the harbour area, the North Sea, the large rivers (e.g. the Maas) and the greenhouses in the *Westland* area. This last area is unique in the world and it is expected that the surface reflectance for these greenhouses will be highly differing from other landcovers.

One of the factors which can influence the datasets is the method used to determine the *Aersol Optical Thickness* (AOT), also called the *Aersol Optical Depth* (AOD). AOD or AOT values are used to describe the amount of aerosols in the air in a certain pixel. These aerosols are small particles of solids and liquids suspended in the atmosphere. The AOT influence has to be separated from the surface reflectance, since it is included in the measurements. There are basically two methods possible for this derision: it can be done by taking a-priori data, for example of another satellite, or by making statistical assumptions. In this research the four datasets used (OMI, TROPOMI, Landsat-8, Sentinel-2) can be split between these two approaches: the OMI surface albedo climatology uses the statistical assumption with respect to the time-series of the observations. It is assumed that in a long enough time-series made over the same location on Earth certain measurements are done where the AOT is very minimal. Sentinel-2 also uses statistical assumptions. These assumptions are comprising of certain threshold values used in determining certain pixels in the obtained images. These pixels are later used in order to derive the AOT. The TROPOMI dataset uses a-priori data in the form of the surface albedo dataset of OMI. This leads to the possibility of determining the AOT since the surface albedo is assumed to be known. Landsat-8 also uses a-priori data in the form of a dataset obtained by a different satellite, called MODIS, in order to correct for the atmospheric effects.

Since the datasets used in this research (the OMI surface albedo database grid, TROPOMI, Sentinel-2 and Landsat-8 datasets) all have very different spatial resolutions, it is important to create regridded versions of all datasets on the same grid with the same resolution. The procedure for doing this is to choose the grid of the TROPOMI data as the target grid. So the OMI dataset and the Sentinel-2 dataset have to be regridded to this TROPOMI grid. The OMI grid has larger pixels, so for this dataset the data itself will not change, the pixels will just be divided into smaller pixels. For the Sentinel-2 dataset the procedure will be different, since its pixels are much smaller than the gridcells of the intended grid. This has to be done by determining which pixels are inside the TROPOMI pixel and then averaging these pixel values for one of the TROPOMI pixels.

When these three datasets are available on TROPOMI resolution, it is possible to look at the differences between the used OMI surface albedo dataset and the available Sentinel-2 dataset. These differences can be visualised in different ways, as absolute or relative difference, on a map and in boxplots etc. When these differences are known it will be possible to estimate the magnitude of the consequences for the final NO_2 product when different a-priori data is used.

The case-study utilises two different periods for which the data was downloaded: the first period, called the *April* period, is the 21$^{\text{st}}$ of April 2018. On this day the two high resolution surface reflectance instruments, Sentinel-2 and Landsat-8, had an overpass over the investigated area and the sky was also cloud-free. This was also the first cloudless day with similar overpasses for which the Sentinel-2 Level-2 dataset was available, since this is only fairly recently become available. The second period, called the *May* period, consists of two days. These days are the 6$^{\text{th}}$ of May for Sentinel-2 and the 7$^{\text{th}}$ of May for Landsat-8. These two days were both cloud free. The overpass times were also similar.

The Level-2 surface reflectance availability of the two high resolution datasets is very limited at the time of this research, especially for Sentinel-2. When the other requirements are taken into consideration, the requirement of the chosen date being cloud free and a similar overpass time, a very limited number of options is left. This is the reason that the May dataset consists of two different days.

This thesis will start with a chapter which covers the procedure which is used in retrieving the NO_2 product. This chapter will also show which dates are used and which specific wavelength-bands are used. The next chapter gives information about the high resolution datasets, Sentinel-2 and Landsat-8. The comparison of the Sentinel-2 and Landsat-8 datasets is also present in this chapter. In the following chapter all datasets are put onto the same grid. This grid is the target TROPOMI grid. In this chapter the comparisons of the present case and the possibility of the high resolution input data are compared. In the last chapter a *Look-Up-Table* (LUT) is created using the *Doubling Adding KNMI* (DAK) radiative transfer model. This LUT is then used in order to calculate *Air Mass Factor* (AMF) values. These AMFs are used in the final stages of deriving the NO_2 tropospheric column. By using the currently used albedo dataset and the two alternative surface reflectance datasets in order to calculate AMF values, these can be compared.

2 NO_2 retrieval

2.1 NO_x Chemistry

NO and NO_2, together called NO_x, are atmospheric species which are involved in a large number of trace gas cycles. Two of these cycles are for example the levels of OH and tropospheric ozone (O_3). Volatile Organic Compounds (VOC) are also influenced by NO_x levels [9].

NO_x is primarily emitted in the form of NO. In the atmosphere, ozone and NO react rapidly and will form NO_2. Under the influence of (sun)light, this NO_2 is photolysed in NO. This leads to an equilibrium during daytime between NO & NO_2. NO_2 also forms nitric acid, one of the main components of acid rain, after reacting with OH and NO_3. These processes are shown in the following figure 2.1 [9]:

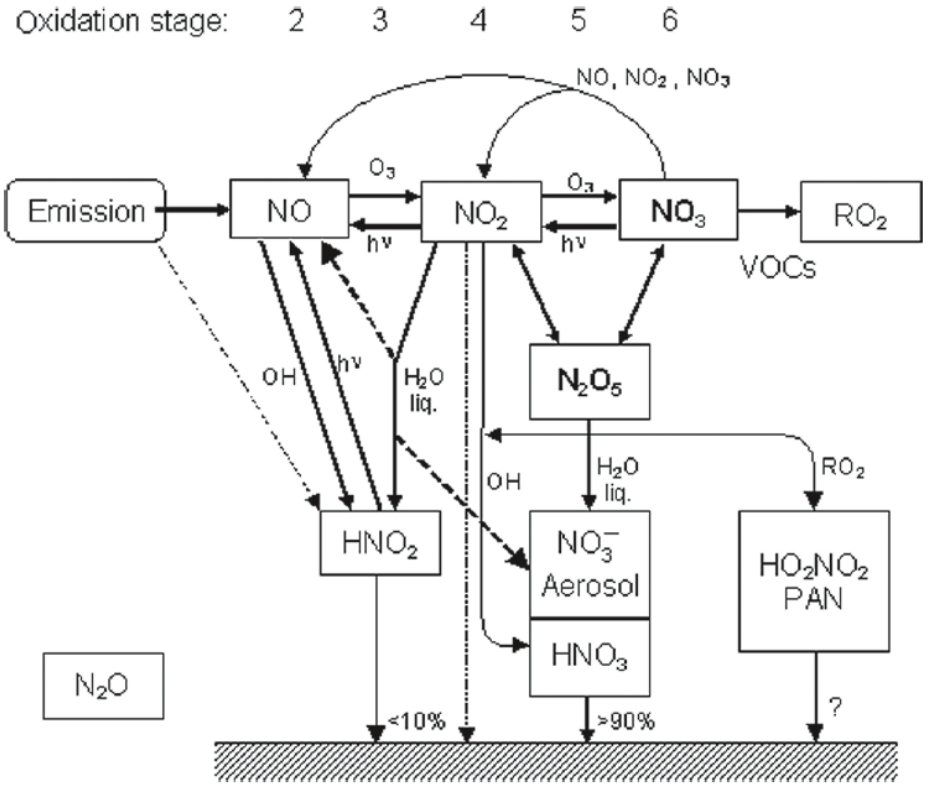

Figure 2.1: Overview of NO_x reaction schemes (Platt & Stutz, 2008).

While figure 2.1 shows a number of important reaction schemes, it is a simplified representation of the reaction in the atmosphere. A number of additional reactions create NO_2 from NO without the need for tropospheric ozone being present. The simple reaction, with HO_2, in a 'clean' atmosphere is [9]:

$$NO + HO_2 \rightarrow NO_2 + OH$$

It is important to note that HO_2 also reacts with ozone, leading to the destruction of ozone.

Without the influence of sunlight (at night) NO_3 plays an important role in the atmosphere. This NO_3 is formed by the following reaction:

$$NO_2 + O_3 \rightarrow NO_3 + O_2$$

During the day this NO_3 is virtually entirely destroyed [9]:

$$NO_3 + hv \rightarrow NO + O_2 \rightarrow NO_2 + O$$

2.2 Retrieval technique

The NO_2 retrieval in this research is done using passive remote sensing techniques. Passive remote sensing refers to the fact that the sensors don't have their own source of light for which they detect the reflection, but they rely on an outside source of light, in most cases the sun. The advantage of the use of sunlight is that the instrument does not have to provide the energy needed to make the measurements.

The sun's radiation directed towards the Earth is then reflected by the Earth's surface. A part of this reflected radiation is directed at the measurement instrument, and is thus picked up. However, the sunlight is not just reflected by the surface of the Earth, it is also affected by the atmosphere. The radiation is scattered and absorbed by atmospheric molecules. One of these influencing atmospheric compounds is NO_2. When the measurements are used for calculations in which the other influencers are sufficiently known the NO_2 retrieval can be done. The final wanted outcome is in this case the *Tropospheric NO_2 column*.

The measurements made used for NO_2 retrievals are made in the ultraviolet and visible parts of electromagnetic spectrum. The needed wavelengths are roughly between 340 and 600 nm, but the optimal retrieval is between 425 and 450 nm [10].

The technique used to retrieve NO_2 is called DOAS fitting. DOAS stands for *Differential Optical Absorption Spectroscopy*. The technique is used for retrieving trace gas abundances. It can be used in two main set-ups, passive and active. In this research the focus is on passive instruments. The technique is based on the law of *Lambert-Beer*, which describes the attenuation of light by the properties of the materials through which it is travelling [9]:

$$I(\lambda) = I_0(\lambda) * exp(-\sigma(\lambda) * c * L)$$

Where:

$I_0(\lambda)$: initial intensity radiation
$I(\lambda)$: radiation intensity
$\sigma(\lambda)$: absorption cross-section
λ : wavelength
c : concentration
L : light path length

The Lambert-Beer formula above contains different variables which are known or can be measured. The initial radation intensity, $I_0(\lambda)$ for example is the radiation coming directly from the sun. This can be measured with high precision. The measured radiation intensity can be described as $I(\lambda)$. $\sigma(\lambda)$, the absorption cross-section is characteristic for atmospheric compounds. When the light-path is assumed to be known, these can be used to determine the concentration of different atmospheric constituents. The final formula used for this calculation looks as follows :

$$ln(\frac{I_0(\lambda)}{I(\lambda)}) = P(\lambda) + \sigma^*_{NO_2}(\lambda) * N^S_{NO_2} + \sigma^*_{O_3}(\lambda) * N^S_{O_3} + \sigma^*_{HCHO}(\lambda) * N^S_{HCHO} + ...$$

Where:

$I_0(\lambda)$: initial intensity radiation
$I(\lambda)$: radiation intensity
$P(\lambda)$: the polynomial fit
$\sigma^*_x(\lambda)$: differential absorption cross-section of constituent x
λ : wavelength
N^S_x : slant column density of constituent x

The formula above shows that when the polynomial fit has been taken out, the remaining measurements can be attributed to different compounds. This is done by taking the (known from experiments) differential absorption cross-sections and than using the most appropriate slant column densities until the best fit is obtained.

The outcomes of the DOAS fitting procedure are known as *Total Slant Columns*. The fact that it is a *Slant* column is because the outcomes of the column densities is the amount of the atmospheric

compound measured by the reflected light towards the satellite, which is often not directly above the observed area, but in an angle, the *Viewing Angle*. The difference between slant and vertical columns is illustrated in a simple manner in figure 2.2.

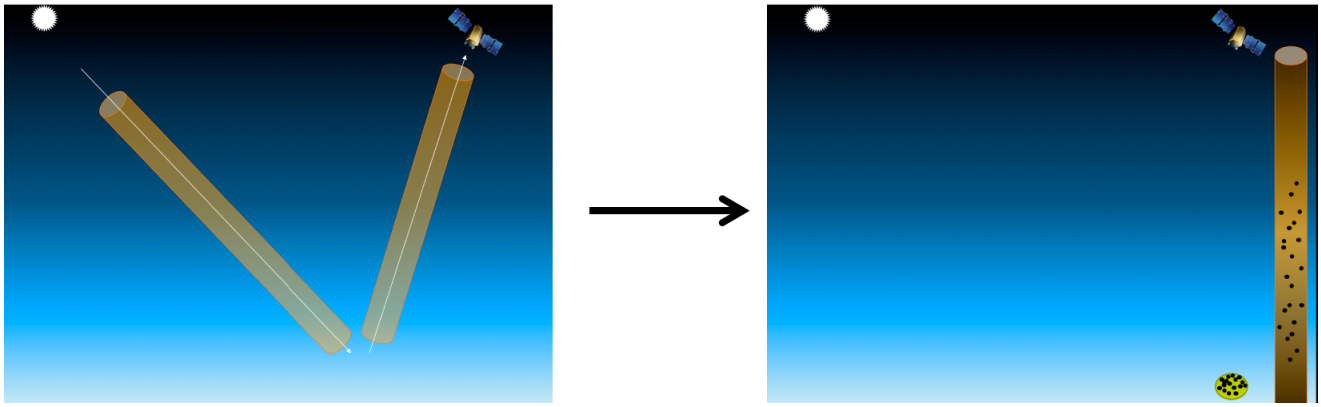

Figure 2.2: Slant (left) and vertical column (right) densities

The slant column which has been derived from the DOAS fit is the *Total* slant column. This means it contains all of the specific compound in the slant column for the entire atmosphere. This research focusses on air quality applications (primarily NO_2), which are specifically interested in the *Tropospheric Column*. This is obtainable by removing the stratospheric slant column.

In figure 2.3 the steps taken in order to obtain the final NO_2 vertical column is shown. This requires the application of the *Air Mass Factor* (AMF). The Air Mass Factor is the result of a formula which shows the connection between the vertical and the slant column densities:

$$AMF = \frac{N^S}{N^V} = \frac{\int n(z)m(z)dz}{\int n(z)dz}$$

Where:

AMF : Air Mass Factor
N^S : slant column density
N^V : vertical column density
$n(z)$: vertical trace gas profile
$m(z)$: box-AMF

This step requires a-priori data input, and this is the step which could be improved. Therefore this research focusses on the a-priori input data required to obtain the final NO_2 product.

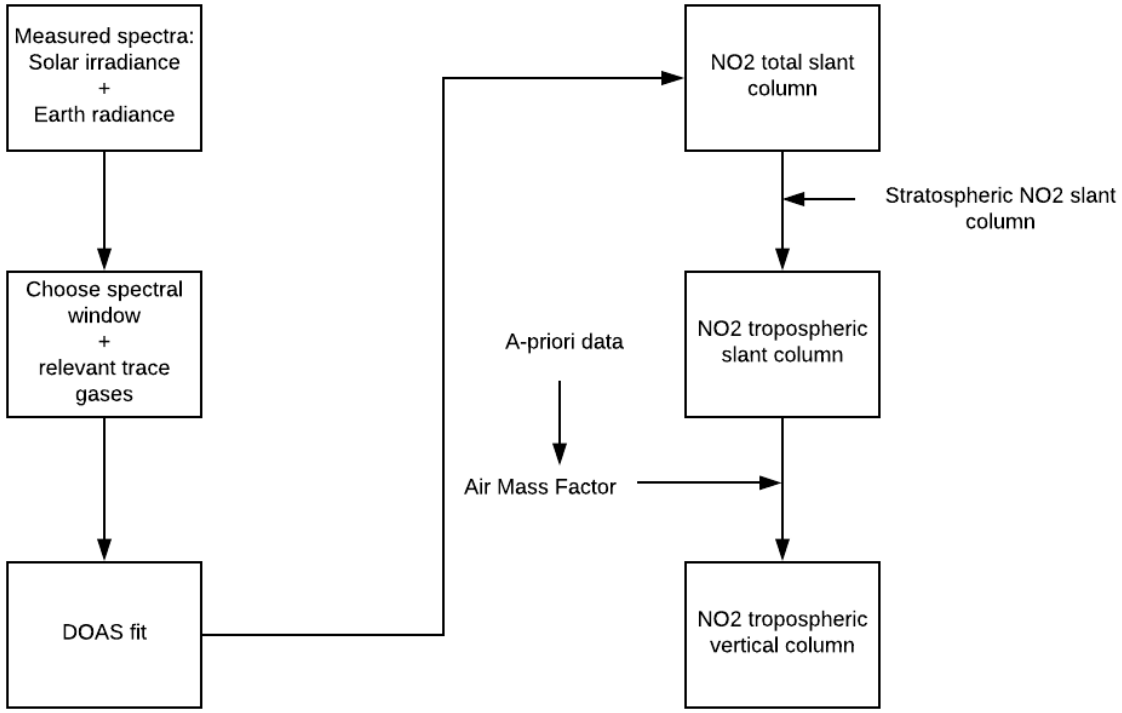

Figure 2.3: Flow chart tropospheric NO2 retrieval

2.3 Optical Properties of the Surface

Passive remote sensing UV-VIS instruments detect reflected sunlight. The initial measurements contain atmospheric influences and are therefore called *Top Of Atmosphere* datasets. When this atmospheric influence has been corrected for, the dataset is called a *Bottom Of Atmosphere* dataset, such as the *Surface Reflectance*. In the next chapter the atmospheric correction algorithms for all the used datasets will be discussed.

Albedo, which comes from the Latin word for whiteness, refers to the amount of diffuse reflection of radiation as a ratio of the total solar radiation. This value is one-dimensional and in (most) radiative transfer models, which describe the interaction of solar radiation with the Earth's atmosphere, the surface is described by an albedo value. Albedo is a scalar between zero and one, where zero refers to a black body, while a value of one corresponds to a perfectly reflecting body. Albedo datasets are often made using longer periods of measurements, since the angle dependencies of surface reflectance are not wanted in albedo products. By using longer periods and averaging out the measurements, these angle dependencies are less prominent. One of the datasets in this research is an albedo dataset, the OMI LER albedo climatology. LER stands for *Lambertian-Equivalent Reflectivity*, and means that the surfaces are assumed to be isotropically reflecting. In other words, the reflected radiation is described by Lambert's cosine law. Therefore, there are no angular dependencies [11].

However, in most remote sensing applications this assumption is not valid. The surfaces do not exhibit Lambertian reflection, and angular dependencies play a role in the reflectance. This angular dependent reflection behaviour can be described using a *Bidirectional reflectance distribution function* (BRDF). This function uses a small number of variables to describe the relation between the magnitude and the direction of incoming solar radiation (sunlight) and the magnitude and direction of the scattered light. BRDF is dependent mostly on the surface type and the spatial resolution of the observations. This function becomes more important when this resolution becomes higher, since smaller pixels lead to an averaging out of high angle dependencies [12]. A BRDF is also dependent on the orientation of the measurement. This orientation can be described by the *Solar Zenith Angle*, the *Viewing Zenith Angle*

and the *Relative Azimuth Angle* (which can all be seen in figure 2.4).

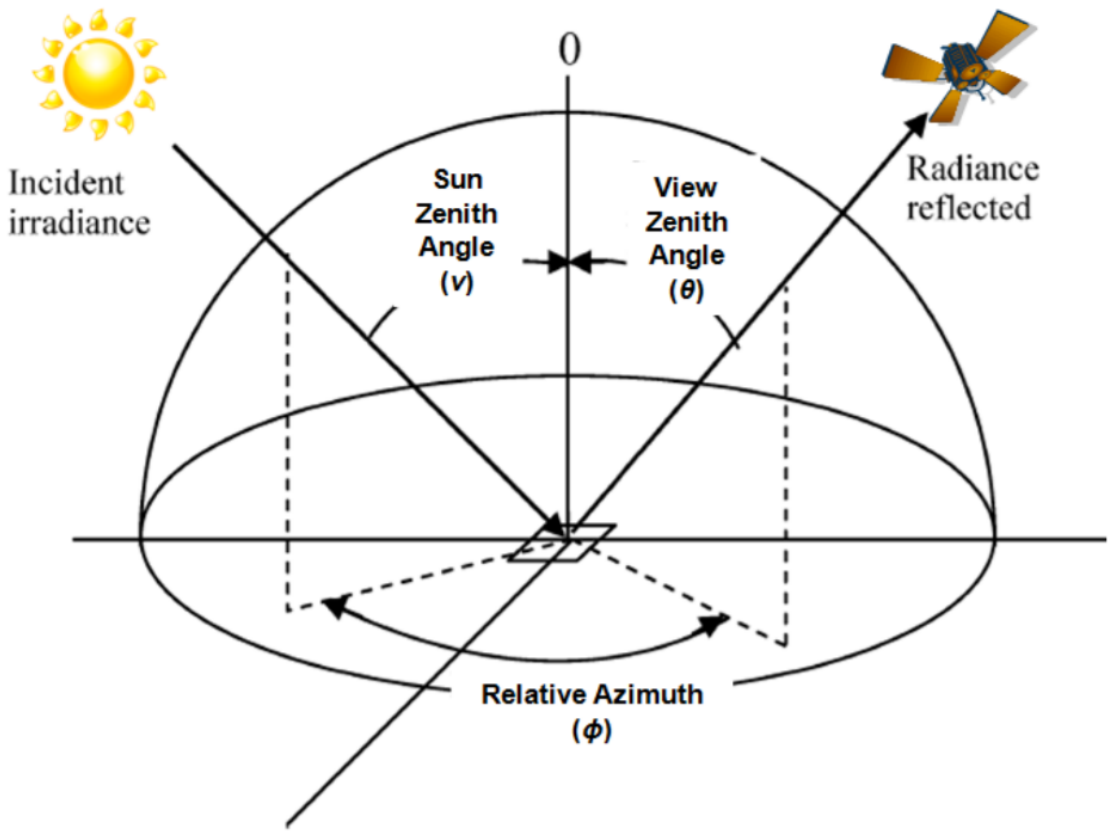

Figure 2.4: The Solar Zenith Angle (v), Viewing Zenith Angle (θ) and the Relative Azimuth Angle (ϕ) in passive satellite instruments (McCamley, 2014).

The fact that BRDFs are dependent on the spatial resolution, as well as the pixel location (which changes every overpass of a satellite), the orientation of the instrument & the sun, make a BRDF impractical. Also the shape of a BRDF changes depending on the terrain. An alternative to the BRDF is called the *surface reflectance*.

In this research surface reflectance is interpreted as follows: for a given radiance observation of a certain pixel with cloud free conditions, the surface reflectance is equal to the (Lambertian) surface albedo which is needed to match the modelled radiance in the radiative transfer model. An assumption is that the atmospheric influence have been modelled ideally.

Surface reflectance is, just like albedo, a scalar between zero and one, where zero means all incoming radiation is absorbed and one means all radiation is reflected. Two of the datasets in this research are surface reflectance datasets: the Sentinel-2 and Landsat-8 datasets.

The procedure used in retrieving the NO_2, together with the chemistry behind NO_2 in the atmosphere has now been discussed. Also the way the surface reacts to incoming sunlight and ways to describe its reflection are described. The next chapter will describe and compare two of the used datasets in this research *Sentinel-2* & *Landsat-8*. After this the third used albedo dataset is described, the OMI LER albedo climatology.

3 Surface Reflectance Datasets

The high resolution surface reflectance dataset which is used in this research is derived from the Sentinel-2 ESA mission. In order to estimate the accuracy and precision and to be able to make any statements about these properties of the Sentinel-2 data, it is important to intercompare this dataset with another dataset. In this research the dataset derived by NASA's Landsat-8 mission was chosen for this purpose.

3.1 Sentinel-2 surface reflectance product & Atmospheric correction algorithm

ESA developed the Sentinel-2 Earth observation mission as a part of the Copernicus Programme. The goal of the mission was to observe the Earth and to create data usable for services like land cover determination etc. [13]. The mission is comprised of two identical satellites, named Sentinel-2A and Sentinel-2B. Two additional satellites are under construction [14]. These satellite orbits are 180° out of phase with each other. This serves the goal of having a high revisit time, so the time period between two observations of the same area is short. This revisit time is approximately ten days for the equator per satellite, so five days for both satellites together. For mid-latitudes this revisit time is shorter, since the overpasses overlap at these latitudes. This leads to a revisit time for mid-latitudes of only two days or sometimes even less for both satellites together [13]. Sentinel-2 has 13 distinct different bands with varying wavelengths. These wavelengths can be seen in figure 3.1.

S2 Band		Wavelength (min-max)	Res. (m)
1	C/A	0.421 - 0.457	60
2	Blue	0.439 - 0.535	10
3	Green	0.537 - 0.582	10
4	Red	0.646 - 0.685	10
5	VRE	0.694 - 0.714	20
6	VRE	0.731 - 0.749	20
7	VRE	0.768 - 0.796	20
8	NIR	0.767 - 0.908	10
8a	NIR	0.848 - 0.881	20
9	WV	0.931 - 0.958	60
10	Cirrus	1.338 - 1.414	60
11	SWIR	1.539 - 1.681	20
12	SWIR	2.072 - 2.312	20

Figure 3.1: Sentinel-2's bands and the corresponding wavelengths

The direct surface reflectance measurements are purely the intensity of the reflected electromagnetic radiation which can be measured by the instrument. This intensity is called the *Top Of Atmosphere* (TOA) surface reflectance, since the effects of the atmosphere are still present in the data. These atmospheric effects include a lot of different influencers, e.g. clouds and aerosols. These influences lead to different reflectance values for the same areas at different times. Therefore for a lot of uses these effects have to be eliminated as thoroughly as possible.

In the case of Sentinel-2 surface reflectance products, the TOA measurements are part of the so-called *Level-1C* product. This is the first level of processing done with the original data (sometimes called Level-0). Level-1 products can be processed using different algorithms in order to create a Level-2 product, in the case of Sentinel-2 *Level-2A*. Level-2 surface reflectance products show the surface reflectance for *Bottom of Atmosphere*, so with the atmospheric influences filtered out as much as possible.

Sentinel-2's Level-2A algorithm comprises of a scene-classification and an atmospheric correction applied to the *Top of atmosphere* Level-1 data. The created Level-2A product has different outputs: A Bottom-of-atmosphere reflectance product, an *Aerosol Optical Thickness* (AOT) map, a *Water Vapour* (WV) map, a Scene Classification map (SCM). *Quality Indicators* (QI) are also present. These show the probabilities of pixels to include snow and clouds.

The Level-2A algorithm is entirely based on threshold tests. These tests use the reflectance values at Top Of Atmosphere (Level-1A) as input. These threshold values were determined using extensive testing. The Level-2A algorithm can be divided into different parts. The first part corrects for cirrus clouds. The second part works tightly together with this cirrus cloud correction part, and comprises of a scene classification module. Part three is the part of the algorithm where the type and visibility (or Optical Thickness) of the atmosphere is determined. Since the data in this paper is very sensitive to aerosols this part will be explained more thoroughly:

An input visibility is needed in order to run this algorithm. This user-defined visibility is by default 20 km. The algorithm can used in different cases. In the first case, in a specific scene area of known reflectance behaviour are present, water bodies or so called *Dark Dense Vegetation* (DDV) pixels (even though other dark areas can be included in the term DDV). These areas of known reflectance are determined in the following manner: The algorithm, Sen2Cor, uses the data of Sentinel-2 itself to determine DDV pixels. It uses a modification of the method proposed in 1988 by Kaufman & Sendra [15]. The assumptions needed for this method are that the variations in the AOT have a negligible influence in the *Short Wave Infrared* (SWIR) part of the electromagnetic spectrum. This part is obtained in Band-12 with Sentinel-2. The starting visibility is used to retrieve the TOA reflectance for Band-12. The next step is to select the pixels with a surface reflectance between 1% and 5% and a *Normalized Difference Vegetation Index* (NDVI) of larger than 0.1 as the DDV pixels. This NDVI is determined by the following calculation:

$$NDVI = \frac{Band8 - Band4}{Band8 + Band4}$$

The primary reason this NDVI value is used since it is effective in determining highly reflective vegetation pixels. Band-8 is the near-infrared band of Sentinel-2. In this part of the electromagnetic spectrum reflectance of green leaves is high, since in this spectral region only small amounts of the sun's energy is absorbed. Band-4, which corresponds to the red part of the visible part of the spectrum, green leaves have a high absorption, so the reflectance is low. The 1% lower threshold for the surface reflectance is needed to exclude water pixels. When less than 1% of the dataset is determined to be usable as dark reference pixels, the high-end threshold is raised to 10% and finally 12% [16].

In the second case, no DDV and soil pixels are present. In this case the reflectance threshold of the highest wavelength band, band-12, is used in an iterative manner so medium brightness pixels can be used as reference. If the scene doesn't include water pixels as well, the third case is implemented and the processing is started with the input visibility.

The water vapour retrieval is done in the fourth part of the algorithm, *Atmospheric Pre-corrected Differential Absorption* (APDA). This part of the algorithm used bands 8A and 9 together, band-8A as reference and band-9 as absorption channel to determine the water vapour content [17].

3.2 Landsat-8 surface reflectance product & Atmospheric correction algorithm

NASA launched the Landsat-8 satellite in February of 2013. As the name suggest, it is the eight satellite in the Landsat series which has been developed with the intention of acquiring satellite imagery of the Earth's surface [18].

Landsat-8 doesn't consist of two sister satellites like Sentinel-2. This leads to a longer revisit time for the same location on the Earth. The revisit time for the entire planet is 16 days. Landsat-8 was placed in an 8-day offset with its predecessor Landsat-7. These satellites together have a shorter revisit time due to this offset, but they don't have the same instruments on board, so it is not a twin constellation like Sentinel-2. The Landsat-8 satellite has 11 distinct wavelength bands, with the first nine being acquired by the *Operational Land Imager* (OLI) instrument. This instrument is the one being focussed on in this research. In figure 3.2 the bands of the OLI instrument can be seen with their corresponding wavelengths and resolution.

When comparing figures 3.1 & 3.2 it can be seen that the bands tend to be very close in terms of wavelengths for both satellites. In this research the focus is on the first bands of bot satellites, the *Coastal Aerosol* band with a wavelength of approximately 443 nm. This wavelength is also the primary source of information for the needed NO_2 product which is derived from TROPOMI (this instrument

Spectral Band	Wavelength	Resolution
Band 1 - Coastal / Aerosol	0.433 – 0.453 µm	30 m
Band 2 - Blue	0.450 – 0.515 µm	30 m
Band 3 - Green	0.525 – 0.600 µm	30 m
Band 4 - Red	0.630 – 0.680 µm	30 m
Band 5 - Near Infrared	0.845 – 0.885 µm	30 m
Band 6 - Short Wavelength Infrared	1.560 – 1.660 µm	30 m
Band 7 - Short Wavelength Infrared	2.100 – 2.300 µm	30 m
Band 8 - Panchromatic	0.500 – 0.680 µm	15 m
Band 9 - Cirrus	1.360 – 1.390 µm	30 m

Figure 3.2: Landsat-8's bands of OLI and the corresponding wavelengths

uses its fourth band, between 405 & 465 nm for the NO_2 product) [19]. More information about this subject can be found in chapter 2.

Just like the measurements made by Sentinel-2, Landsat-8 measures the reflectance which has passed through the atmosphere, the *Top Of Atmosphere* reflectance. This TOA reflectance still has the different influencers in the data, like clouds and aerosols. In order to compare the two high resolution datasets it is important to have the same type of data. Therefore the *Surface Reflectance* Landsat-8 dataset has been chosen, since this has had the atmospheric correction. The Surface Reflectance Landsat-8 dataset comprises of the following files [20]:

- Surface Reflectance data files (Bands 1-7)
- Radiometric Saturation QA Bands
- Surface Reflectance Aerosol QA band
- Level-2 Pixel Quality Assessment Band
- Surface Reflectance metadata file
- Level-1 metadata file
- Level-1 Angle Coefficient file

Landsat-8's atmospheric correction algorithm differs from Sentinel-2 dataset in the fact that it doesn't only take its own measurements as input data. It uses input data, in this case data of MODIS, in order to correct for the atmospheric effects. MODIS stands for *Moderate-resolution Imaging Spectroradiometer*, and is a device aboard the *Terra* and *Aqua* satellites which were launched in 2002. The two satellites together are capable of scanning the entire Earth every one or two days. They make measurements in 36 spectral bands ranging from approximately $0.4\mu m$ to $14.4\mu m$ [21]. One of the available data products, which is used by the Landsat-8 algorithm, is a daily aerosol product. This product has a spatial resolution of 10 km x 10 km [22]. Landsat-8's first band ($0.443\mu m$), designated as the *Coastal Aerosol Band*, is used to perform aerosol inversion tests. This is used as a check-up for the MODIS input. The algorithm is also dependent on a unique *Radiative Transfer Model* [23].

3.3 Comparison between Sentinel-2 & Landsat-8 surface reflectance products

Both satellite systems are highly regarded in the satellite imaging fields. The two satellites have different algorithms to derive surface reflectance (and hence to perform an atmospheric correction) and this may lead to differences on individual days. Such differences can partly be understood in terms of differences in a-priori data and assumptions made, and partly to instrumental biases. For the purposes of this study it suffices to compare both products and to investigate to which extent the unexplained mutual differences are small/large in comparison to the OMI surface albedo database and to check whether the data which will eventually be used for this research is of sufficient quality. This influences the outcomes of this research directly. For this comparison it is important to take the most comparable datasets for both satellites, which in this case was chosen to be the level-2 datasets, hence on the original grid.

The first step to take before the actual comparison can be done is by simply plotting the datasets in the same manner and to check whether they are broadly comparable. This can be seen in figure 3.6 (Sentinel-2 on the left side and Landsat-8 on the right side) for the April datasets, and for the datasets acquired in May this can be seen in figure 3.7. The conditions for these datasets to be usable for these research are: the days of acquisition had to be cloud free, both satellites had to have visited the area shortly after each other and the *Aerosol Optical Thickness* could not be too high. For this research this led to two different available comparable datasets: the *April* datasets, these datasets were both acquired on the 21st of April 2018 with a difference of only about 20 minutes apart. The other dataset, *May*, was acquired on two different days, the 6th and 7th of may for Sentinel-2 & Landsat-8 respectively. Since the influence of the aerosol optical depth is significant on these outcomes, below the *Aerosol Optical Depth* (AOD) maps of MODIS can be seen, next to the corresponding measurements made at the Cabauw site in the Netherlands (figures 3.3, 3.4 & 3.5).

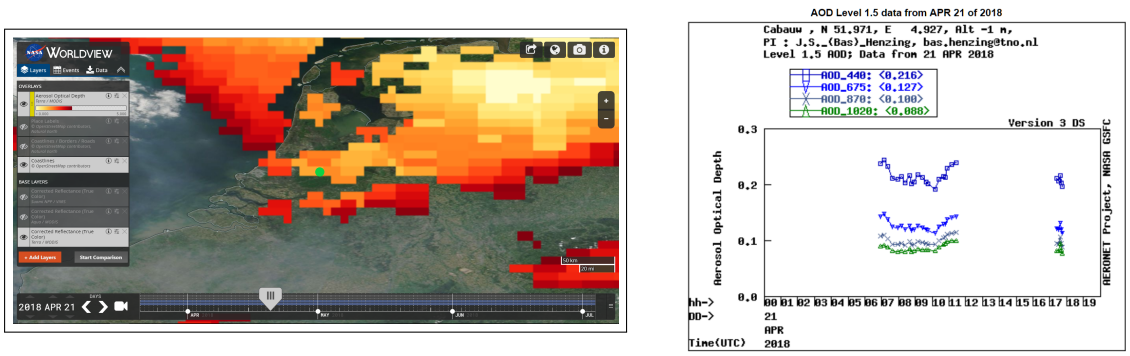

Figure 3.3: MODIS AOD map (left) & Cabauw AOD measurements (right) for April 21. Cabauw's location is represented by the green dot on the MODIS map.

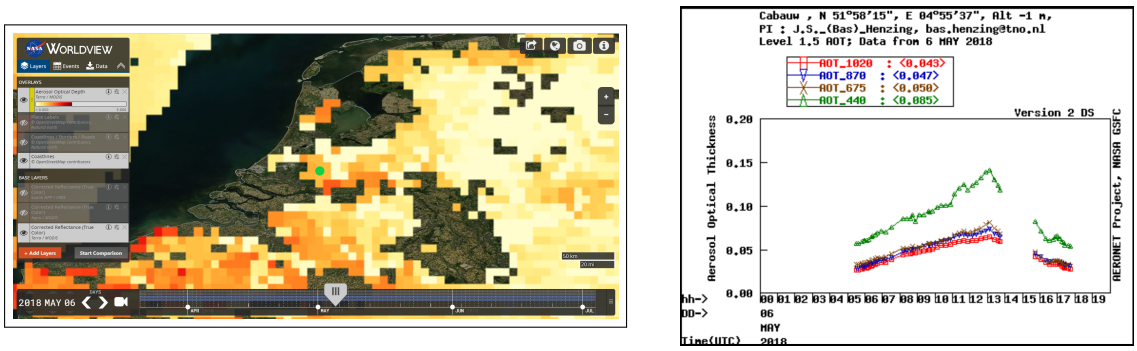

Figure 3.4: MODIS AOD map (left) & Cabauw AOD measurements (right) for May 6. Cabauw's location is represented by the green dot on the MODIS map.

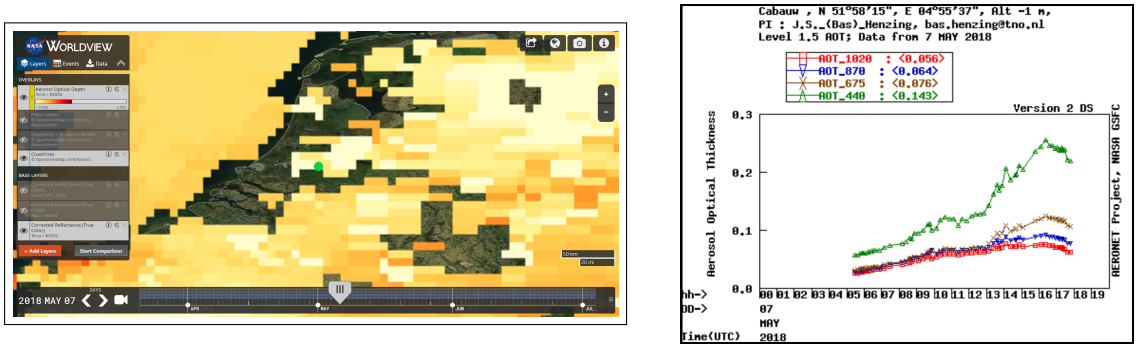

Figure 3.5: MODIS AOD map (left) & Cabauw AOD measurements (right) for May 7. Cabauw's location is represented by the green dot on the MODIS map.

These figures show that the aerosol measurements made by MODIS and at the Cabauw site are comparable. For the 21st of April both MODIS and the Aeronet values are approximately 0.10. The most important conclusion is that for the May dataset, which is taken on two days: May 6 for Sentinel-2 and May 7 for Landsat-8, the aersol values are comparable. MODIS showed 0.08 and 0.03 for the 6th & 7th respectively, while Aeronet showed approximately 0.10 and 0.08 respectively. These differences between the instruments due to the different dates are small, they are within the accuracy of MODIS, which is around 0.05 [24]. Especially when taking into account that the fly-over time for both satellites was around 10:30 am UTC on those dates.

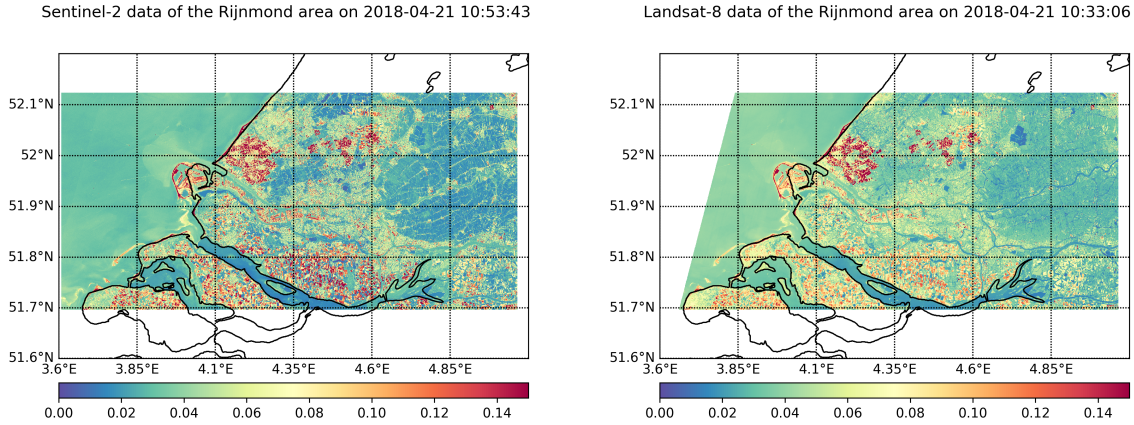

Figure 3.6: Sentinel-2 (left) & Landsat-8 (right) surface reflectance data for Band-1 ($\sim$ 443 nm) for April. Surface reflectance above 0.15 is clipped to this maximum value for better visibility in other regions

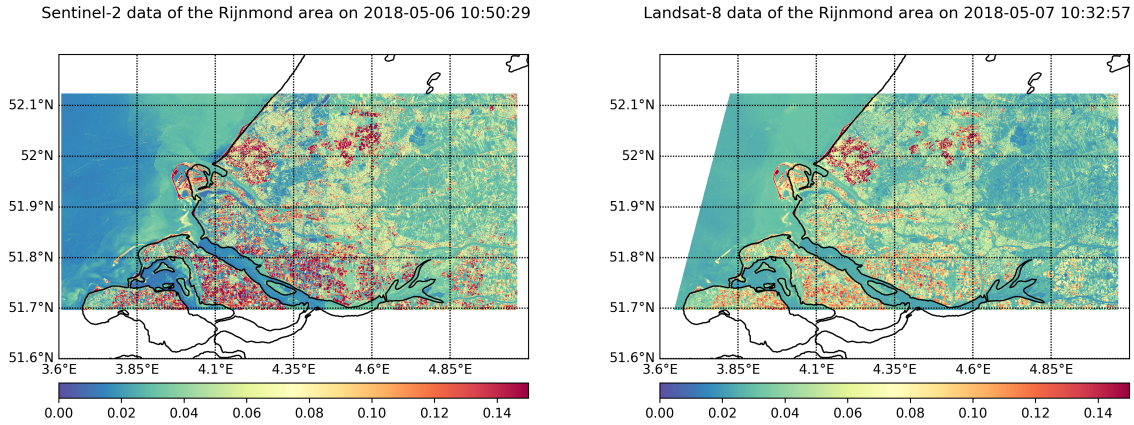

Figure 3.7: Sentinel-2 (left) & Landsat-8 (right) surface reflectance data for Band-1 ($\sim$ 443 nm) for May. Surface reflectance above 0.15 are clipped to this maximum value for better visibility in other regions

The first noticeable difference between figures 3.6 & 3.7 is the higher surface reflectance values for the Landsat-8 datasets in rural parts and above water (i.e. a higher background reflectance), especially for the April datasets. However, the differences in value are not too high. It is also important to take into account that the difference in acquisition time, however short it may be, can cause some difference between the two datasets. This is due to changes between the two acquisition times, the two biggest influencers being: the *Solar Zenith Angle* (SZA) and the *Viewing Angle*. The overpass times, in UTC, for the April dataset, so acquired on the 21st of April, are 10:53:43 for the Sentinel-2 dataset and 10:33:06 for the Landsat-8 dataset. This difference of approximately 20 minutes causes the SZA to differ slightly: 41.11° for Sentinel-2 and 42.27° for Landsat-8. The May dataset, which was acquired over two days, the 6th of May for Sentinel-2 and the 7th of May for Landsat 8, saw roughly equal overpass times, 10:50:29 for Sentinel-2 and 10:32:57 for Landsat-8. The SZA's were slightly smaller (due to the days being later in the year) with 36.60° for Sentinel-2 and 37.38° for Landsat-8.

The atmospheric corrections made in the algorithms of both datasets differed, as can be seen earlier in this chapter. Since these corrections differed in terms of the calculations, but also in terms of input data it has to be noted that these differences will also have an effect on the measurements.

The next comparison which can be made is by making sure the two datasets are regridded to the exact same grid. In this research the Landsat-8 dataset was regridded to the Sentinel-2 grid. The regridding of the Landsat-8 measurements was done using *Python*. The module *SciPy* was used, and specifically the interpolate griddata function, which performed a nearest neighbour interpolation. This approach was chosen since a pixel of Landsat-8 was needed for every pixel of Sentinel-2. Nearest neighbour also saves the extreme values and doesn't average these out. If another type of interpolation was used, for example linear interpolation, local extremes would have become smoothed. Furthermore, this interpolation method is suitable for the final part of this thesis. This part, which will become clear in the next chapter, will have regridded the datasets to a larger pixel-size grid. On this resolution the influence of this decision will have become negligible.

The starting resolutions for both datasets were 60 x 60 metres Band-1, which remained the same. The difference is the fact that the pixels of Landsat-8 are placed directly on top of the Sentinel-2 pixels.

Now the datasets are on the exact same grid, the first comparison is performing a simple subtraction. The results for the April and May datasets can be seen in figures 3.8 & 3.9. These figures can be interpreted as the right figures of figures 3.6 & 3.7 subtracted off of the left figures, so the Landsat-8 dataset subtracted of the Sentinel-2 dataset.

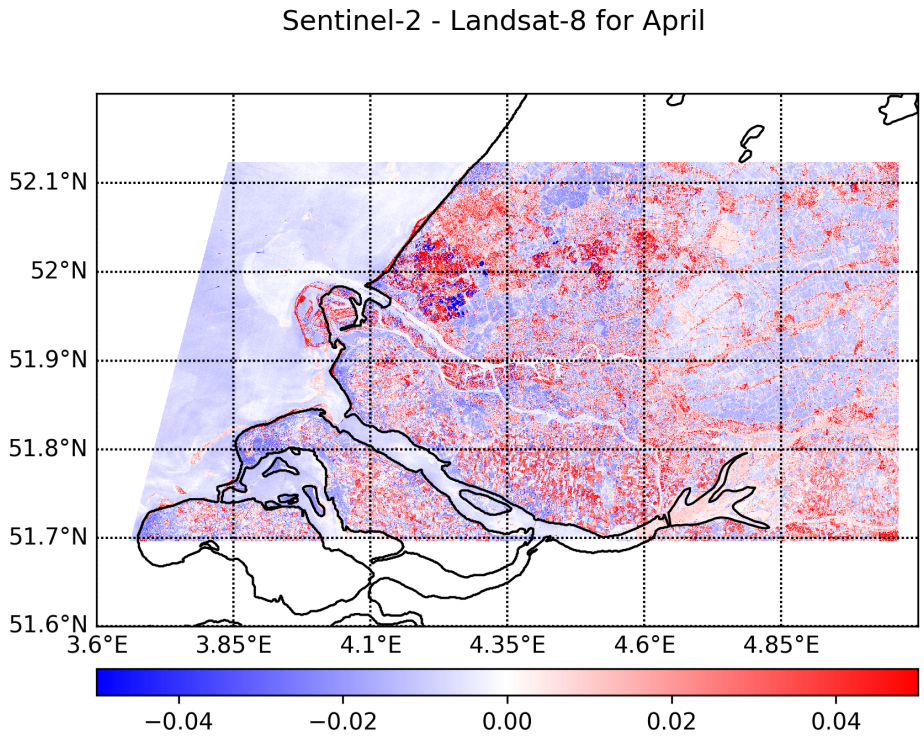

Figure 3.8: Difference of the first band of Landsat-8 and Sentinel-2 for the April datasets

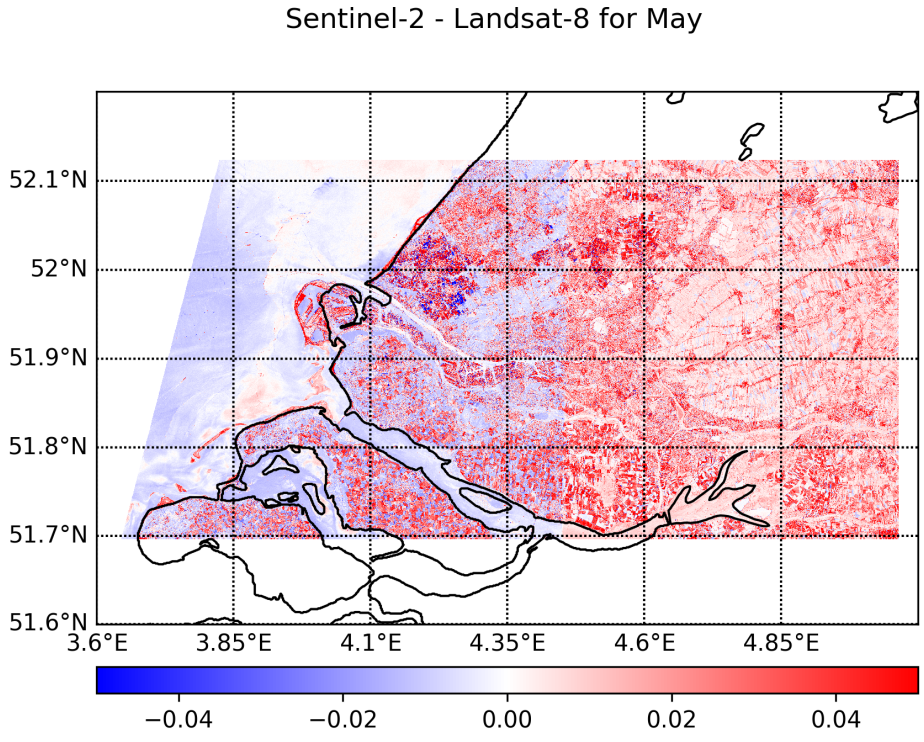

Figure 3.9: Difference of the first band of Landsat-8 and Sentinel-2 for the May datasets

The figures 3.8 & 3.9 show the result when subtracting the first band off of the Landsat-8 dataset off of the Sentinel-2 dataset's first band. Therefore the blue pixels show areas where the surface reflectance of the Landsat-8 dataset is larger and the red pixels show the same for the Sentinel-2 dataset. The water-surfaces are mainly blue, so the reflectance of Sentinel-2 is generally lower for these areas, while the red areas are mostly in the rural parts of the map. This is true for both the April and May datasets.

In this figure a clear inconsistency can be observed between the western and eastern parts of the map, especially for the May dataset. The eastern part of the map show almost exclusively higher values for the Sentinel-2 surface reflectance dataset. This can be explained by the data acquisition of the Sentinel-2 dataset. The Level-2 Sentinel-2 product is divided into Granules (or tiles) which are named using its projection system, which is the UTM (Universal Transverse Mercator)/WGS84 projection. This system contains 60 granules which cover the entire Earth's surface. These tiles have an area of 100x100 km [25]. The processing done to obtain the Level-2 product is done per tile [26]. After this processing the actual data acquisition is done by selecting an area of interest, for which all the necessary granules will be downloaded and 'stitched' together. Since the processing is done independently this process can incite differences inside one area, which is the case for the *May* dataset in this research. These differences tend to be very small (for the May dataset of this research the difference is approximately 0.01), but are nonetheless visible in figure 3.9, since the colour bar is a very small range. Given that the focus areas of this research are all located in the western part of this map this will not lead to any problems. The Sentinel-2 dataset also provided an aerosol optical depth dataset which shows the same inconsistency in exactly the same location. This shows that the inconsistency can possibly be retraced to the difference in Aerosol optical Depth values for the Western and Eastern parts of the map. The figures below, 3.10 & 3.11, show these AOD maps and table 3.1 show the prevailing AOD values for the MODIS dataset (used for Landsat-8) the Sentinel-2 AOD value and the AOD provided by Aeronet. It becomes clear that the values for May are sufficiently smaller than the values for April. The difference between the MODIS (which is used for Landsat-8) and the Sentinel-2 AOT values is larger for the May dataset however. This might explain the larger differences in figure 3.9. The shape of the inconsistency is definitely due tot the Sentinel-2 data being delivered in tiles, since the AOT and difference maps both show the dividing line in the same location. This can be seen in figures 3.10 & 3.11.

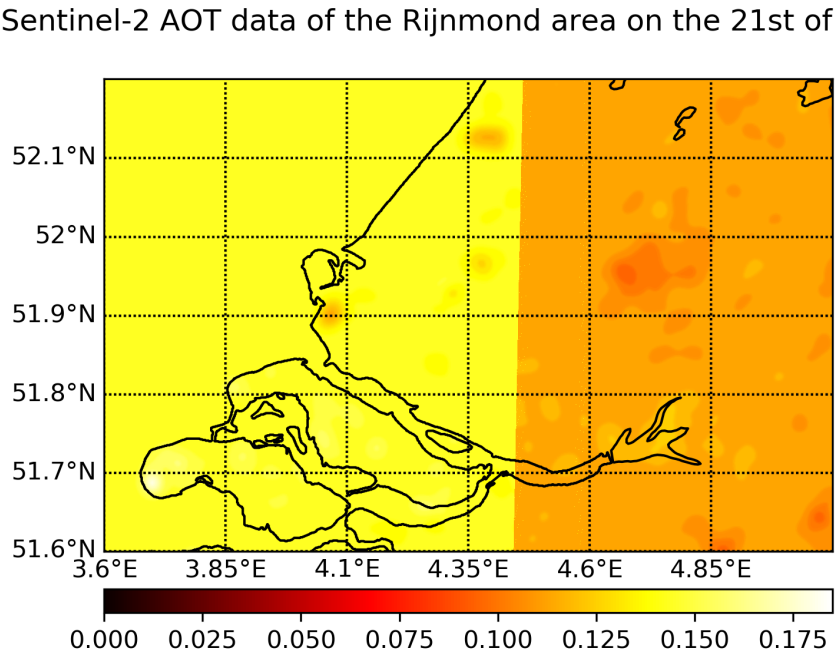

Figure 3.10: Sentinel-2 Aerosol Optical Depth dataset for the Rijnmond area on the 21st of April

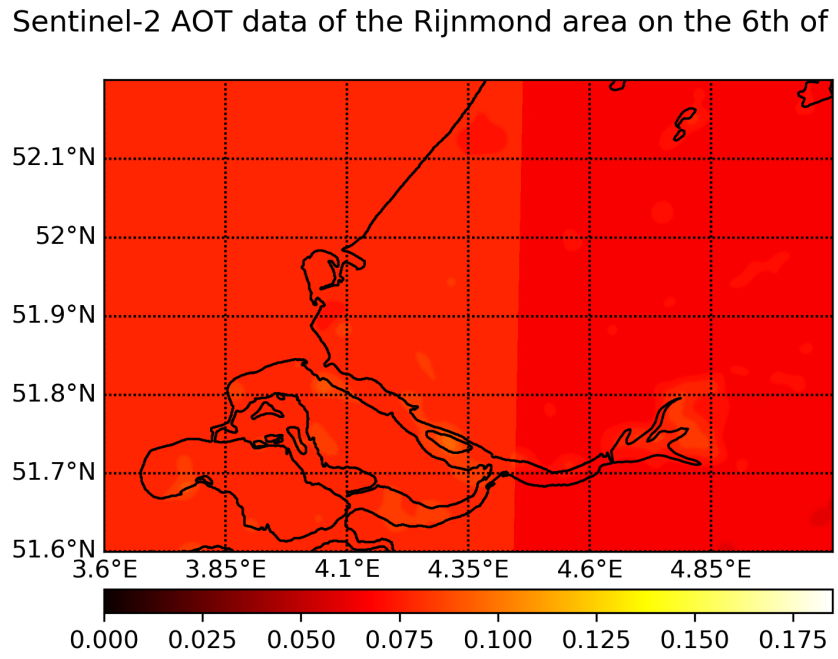

Figure 3.11: Sentinel-2 Aerosol Optical Depth dataset for the Rijnmond area on the 6th of May

	April	May
MODIS	0.120	0.040
Sentinel-2	0.113	0.066
Aeronet	0.174	0.083

Table 3.1: Aerosol optical depth values for the 21st of April & the 6th of May for MODIS, Sentinel-2 and Aeronet

3.3.1 Subsets

After this initial simple subtraction it was decided to define categories for different kinds of terrain which looked to be interesting for this research. Six of these categories were chosen:

- *Greenhouses*, located in the so-called *Westland* in the west of the Netherlands. This area is famous for its high number of greenhouses.
- *Coastal Waters Surface*, an area located in the North Sea, just off the coast.
- *River*, a large chunk of the river *Haringvliet*.
- *Rural*, this subset is located south of Rotterdam and covers the *Hoeksche Waard*.
- *Urban*, this subset covers a very large and urban part of the city of Rotterdam.
- *Industry & Harbour*, this subset consists of the Maasvlakte, an artificial piece of land in the North Sea which is highly industrialised.

The following figure, figure 3.12, shows the regions selected for these six categories (visualised using band-1 of the Sentinel-2 dataset) on the same map as the entire datasets of Sentinel-2 and Landsat-8. The figures below this, figures 3.13 & 3.14 shows all six of the subsets for both Sentinel-2 and Landsat-8 datasets.

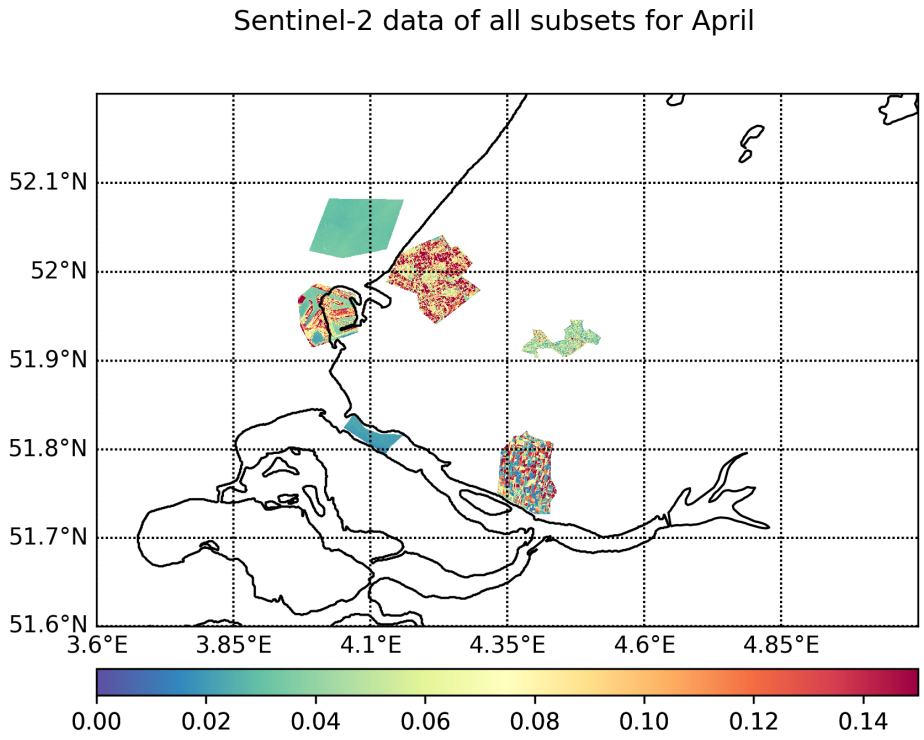

Figure 3.12: All subsets, shown by the Sentinel-2 surface reflectance April dataset.

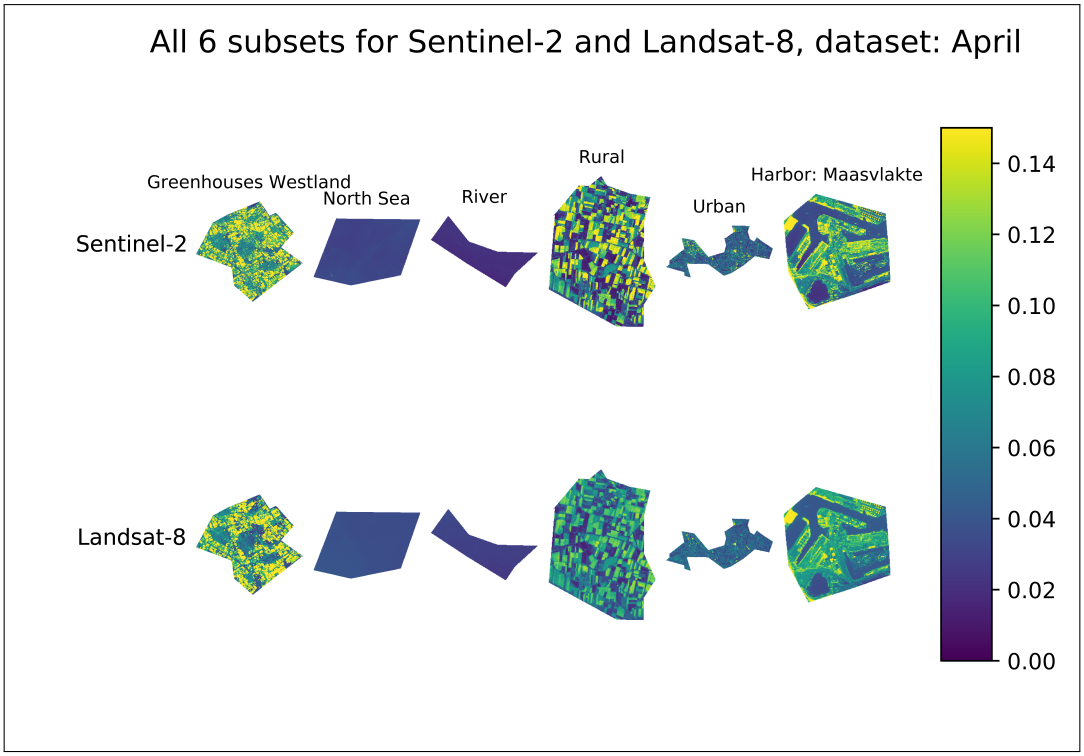

Figure 3.13: All 6 subsets, shown by the Sentinel-2 & Landsat-8 surface reflectance datasets for the 21st of April.

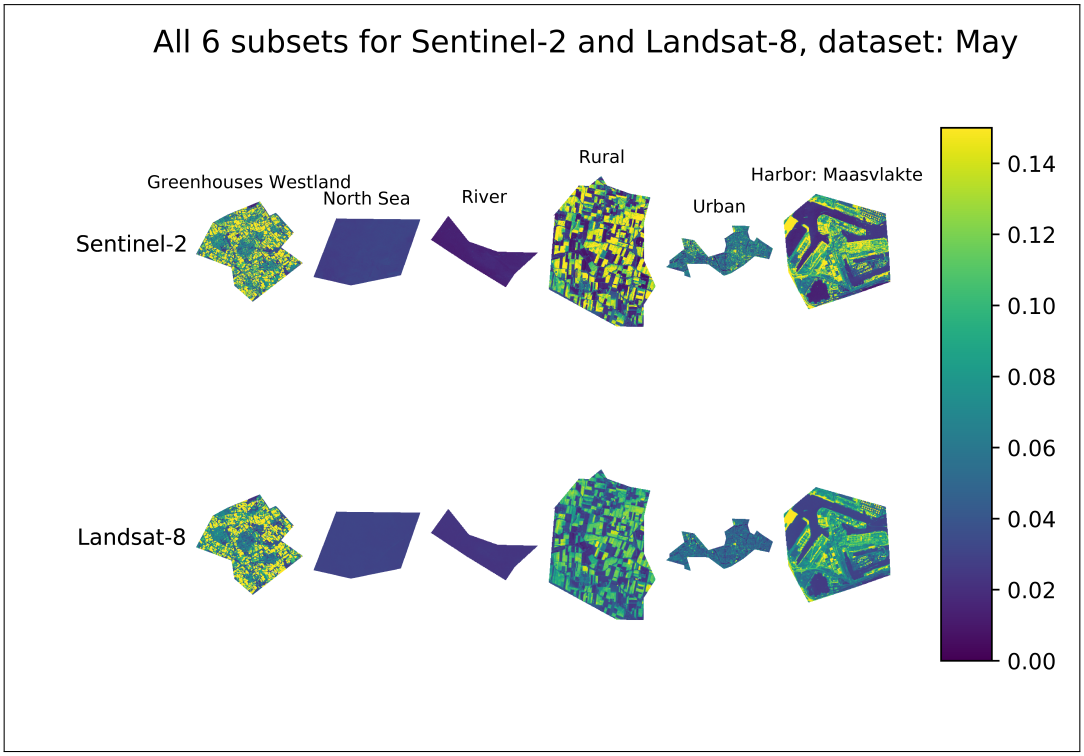

Figure 3.14: All 6 subsets, shown by Sentinel-2 & Landsat-8 surface reflectance datasets for the 6th & 7th of May.

Subsets two until six, so the subsets: North Sea, River, Rural, Urban and Harbor: Maasvlakte, are chosen due to their specific land covers, which can be seen as representative for similar land cover types. The odd one out, in this case the first subset: Greenhouses Westland, is a very specific type of land cover.

This area is covered in greenhouses. These greenhouses lead to a very unique type of reflection of sunlight. This is due to the greenhouses being constructed out of glass, which causes a very high dependence on Solar Zenith angle and viewing angle. This is also closely related to the aforementioned BRDF. It is important to note that this BRDF is not only affected by the angles of the sun and the instrument, but resolution also plays a role. This is especially the case for this very unique greenhouse area. It can be compared to a mirror in regards of the reflection angle.

By making different types of comparisons between the two datasets for these subsets, conclusions of the compatibility of Sentinel-2 and Landsat-8 can be made. The first difference maps which can be made are the simple subtractions, like they were made for the entire map earlier. Just as before, the subtraction was as follows: Sentinel-2 - Landsat-8. This means that in figures 3.15 & 3.16 blue values show where the surface reflectance of Landsat-8 was higher and red where Sentinel-2's values were higher.

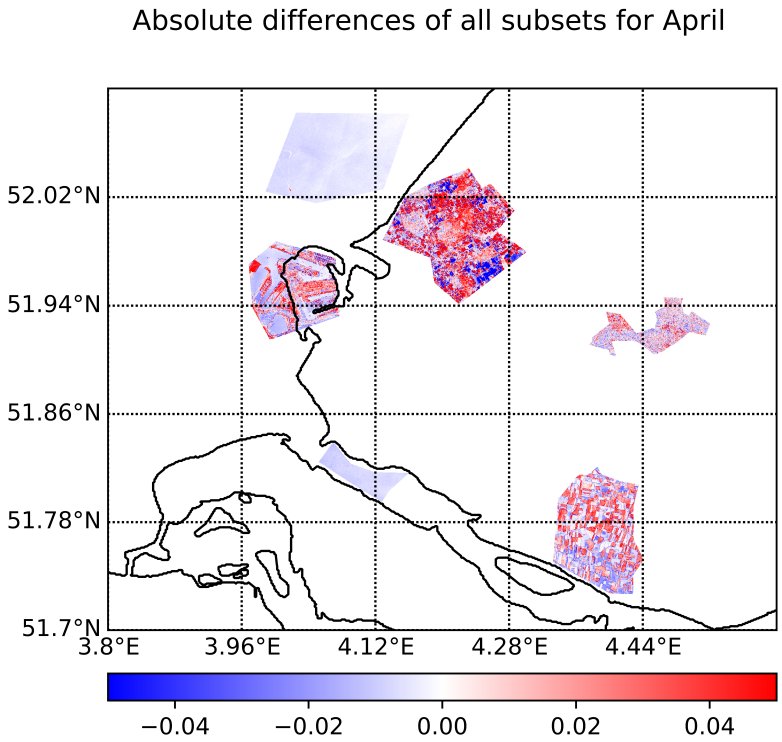

Figure 3.15: Differences of all 6 subsets, Landsat-8 subtracted off of Sentinel-2 , for the April dataset.

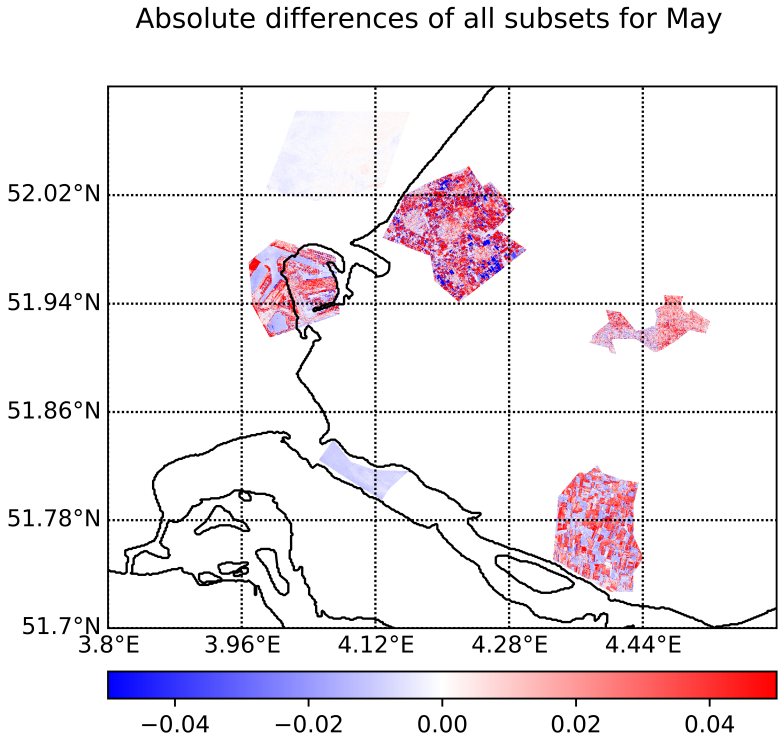

Figure 3.16: Differences of all 6 subsets, Landsat-8 subtracted off of Sentinel-2, for the May dataset.

In these figures a few consistencies can be seen. For both the April and May datasets, the surface reflectance values for the water surfaces appear to have higher values in the Landsat-8 dataset, approximately 0.01. Further, the greenhouses show what was expected, high negative and positive values scattered throughout its area. This corresponds with the idea of a very high dependency on Solar Zenith angle and viewing angle. Also when the surface reflectance values itself are high, differences also tend to be higher.

Apart from a simple subtraction, there are other ways of showing the differences between two datasets. The so-called relative difference. The advantage of this relative difference is that it doesn't prefer one dataset above the other. Another advantage is that generally it leads to fewer extreme values over a region with high values. The formula is as follows:

$$\frac{(A-B)}{0.5*(A+B)}*100\%$$

In this case A and B stand for the dataset of Sentinel-2 and the dataset of Landsat-8 (regriddded to the grid of Sentinel-2). When the differences of the same six subsets are then calculated, figures 3.17 & 3.18 can be created:

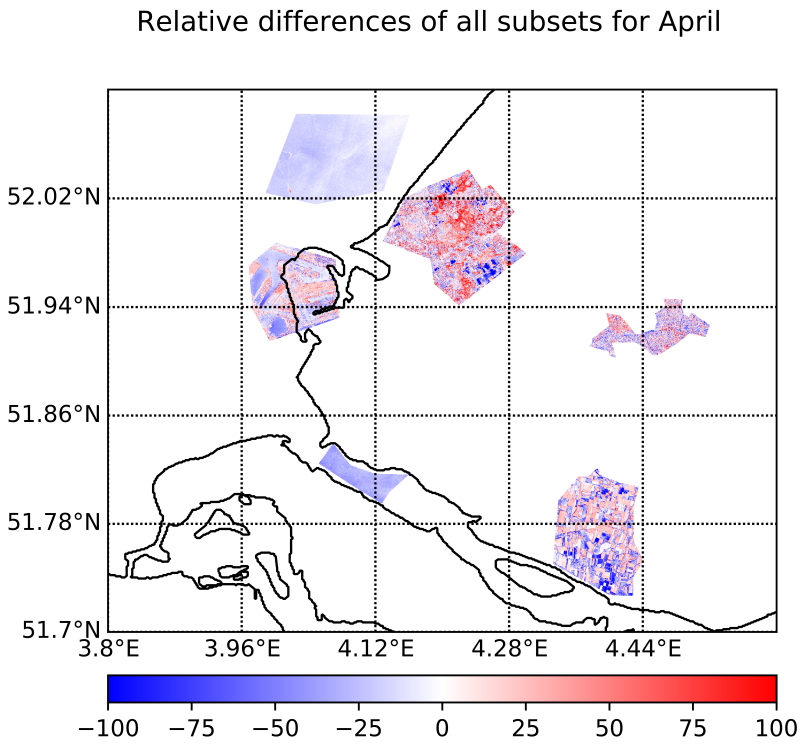

Figure 3.17: Differences of all 6 subsets, Landsat-8 subtracted off of Sentinel-2 , for the April dataset

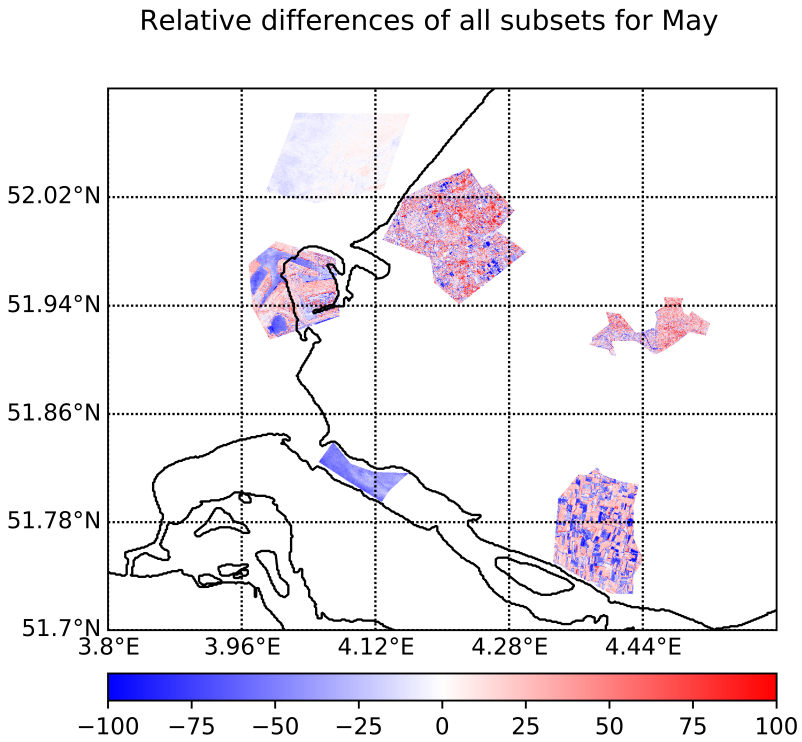

Figure 3.18: Differences of all 6 subsets, Landsat-8 subtracted off of Sentinel-2, for the May dataset

These relative difference maps show that the visible differences between the datasets are almost insignificant above the water surfaces. They also show that the differences are indeed higher above the rural subset. The Westland subset, which has a very high number of greenhouses, shows the same results again, very high differences. However, it also shows that relatively speaking the differences are less significant than for the absolute differences. The urban subset shows higher relative difference values. This was to be expected, since urban areas, Rotterdam in this case, have predominantly in-homogeneous land use, e.g. different types of buildings. This lead to the same outcome as the Westland subset, so higher differences very locally.

Another method of visualising the two datasets together is by making histograms of the surface reflectance in the first bands. When these are plotted in the same figure, any constant inconsistencies can be spotted and some general behaviour might be deducted from the figures. These histograms are shown in figures 3.19 until 3.24.

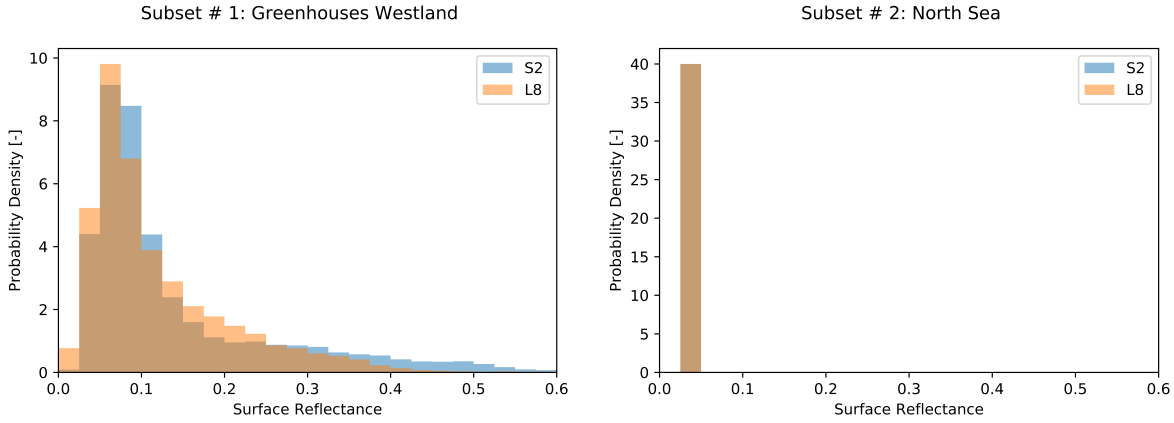

Figure 3.19: Histogram of the surface reflectance of Sentinel-2 (S2) and Landsat-8 (L8) for the April dataset, subsets 1 & 2.

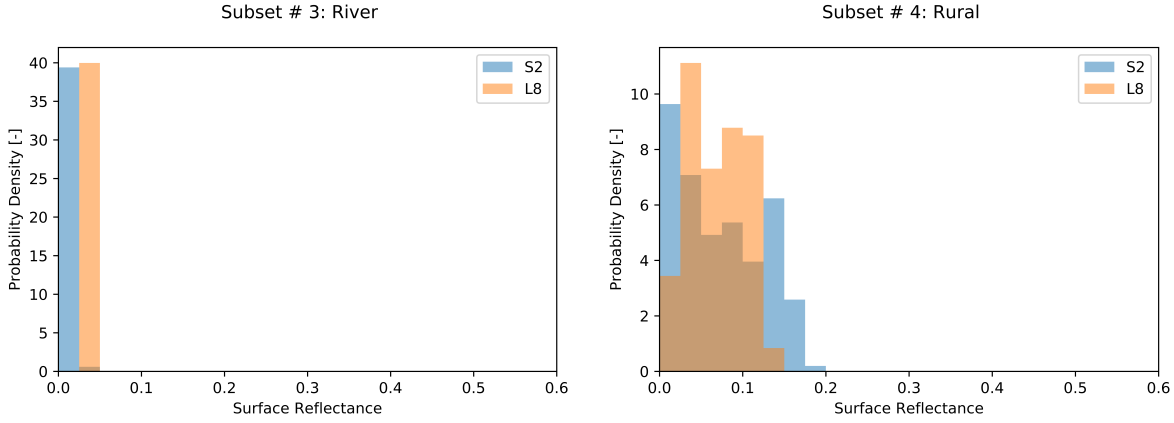

Figure 3.20: Histogram of the surface reflectance of Sentinel-2 (S2) and Landsat-8 (L8) for the April dataset, subsets 3 & 4.

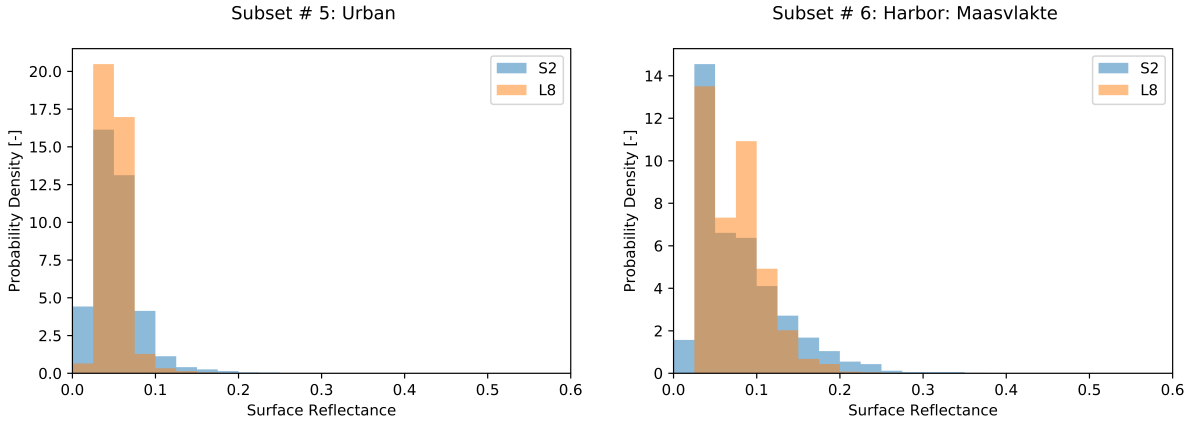

Figure 3.21: Histogram of the surface reflectance of Sentinel-2 (S2) and Landsat-8 (L8) for the April dataset, subsets 5 & 6.

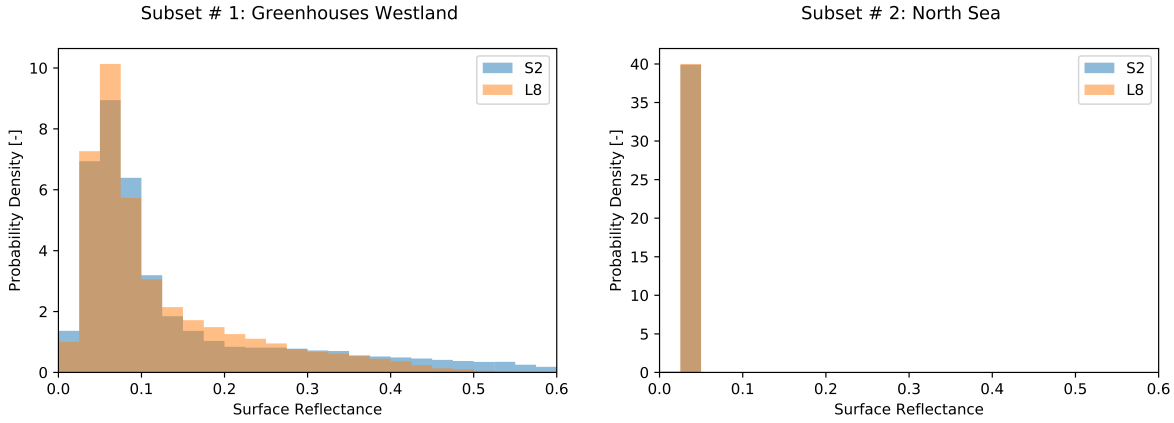

Figure 3.22: Histogram of the surface reflectance of Sentinel-2 (S2) and Landsat-8 (L8) for the May dataset, subsets 1 & 2.

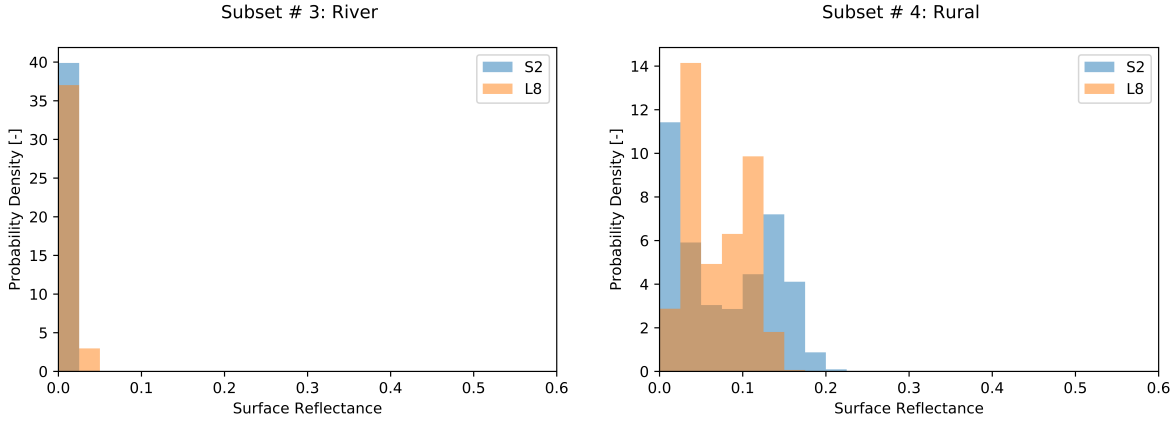

Figure 3.23: Histogram of the surface reflectance of Sentinel-2 (S2) and Landsat-8 (L8) for the May dataset, subsets 3 & 4.

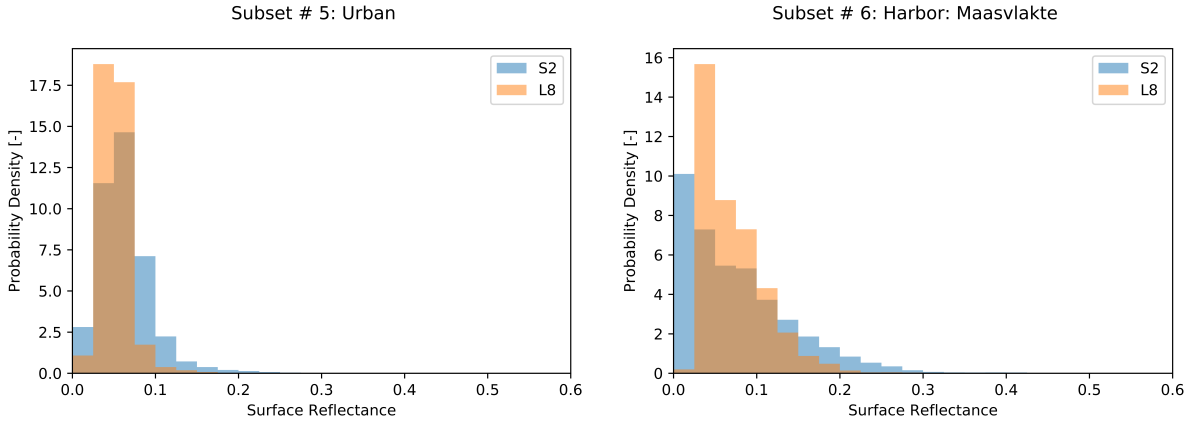

Figure 3.24: Histogram of the surface reflectance of Sentinel-2 (S2) and Landsat-8 (L8) for the May dataset, subsets 5 & 6.

The overall behaviour of the histograms shows that the two datasets are very comparable. They show roughly the same shape for all the subsets and the same differences between the subsets. When looking into detail the differences can be spotted however. The histograms support the conclusions made by looking at the differences, absolute and relative, mapped in the previous figures. The two

water subsets, North Sea and River, show indeed that the values of the two datasets are very close and show almost no variability. Especially the North Sea subset values are almost identical. The absolute difference figures showed that the Landsat-8 values for water surfaces were consistently slightly higher than its Sentinel-2 counterpart. In the histograms this behaviour can be seen very clearly for the River subset. In the May dataset, the river subset shows that the values of Landsat-8 are consistently higher than the Sentinel-2 values. The Westland: Greenhouses dataset shows similar behaviour, although Sentinel-2 shows higher peak values (i.e. the distribution has a longer tail). The rural subsets show a very interesting pattern. For the April dataset both instruments show a bi-modial distribution, while for the May dataset the histograms show a more regular distribution for the Sentinel-2 dataset while the Landsat-8 dataset histogram shows the two peaks very clearly. This can help explain the relatively high differences in this subset. The urban subset, which consisted of the city of Rotterdam, shows comparable values for April and May. The histograms show that the values of Landsat-8 were quite concentrated at certain surface reflectance values, while the Sentinel-2 data was more spread-out over a larger number of surface reflectance values. The Harbour: Maasvlakte dataset shows a similar pattern to the Urban dataset. More low surface reflectance values are present as well as more higher values for the Sentinel-2 dataset.

Apart from difference maps and histograms, boxplots of the surface reflectance differences can also be used to reveal more of the details, figure 3.25.

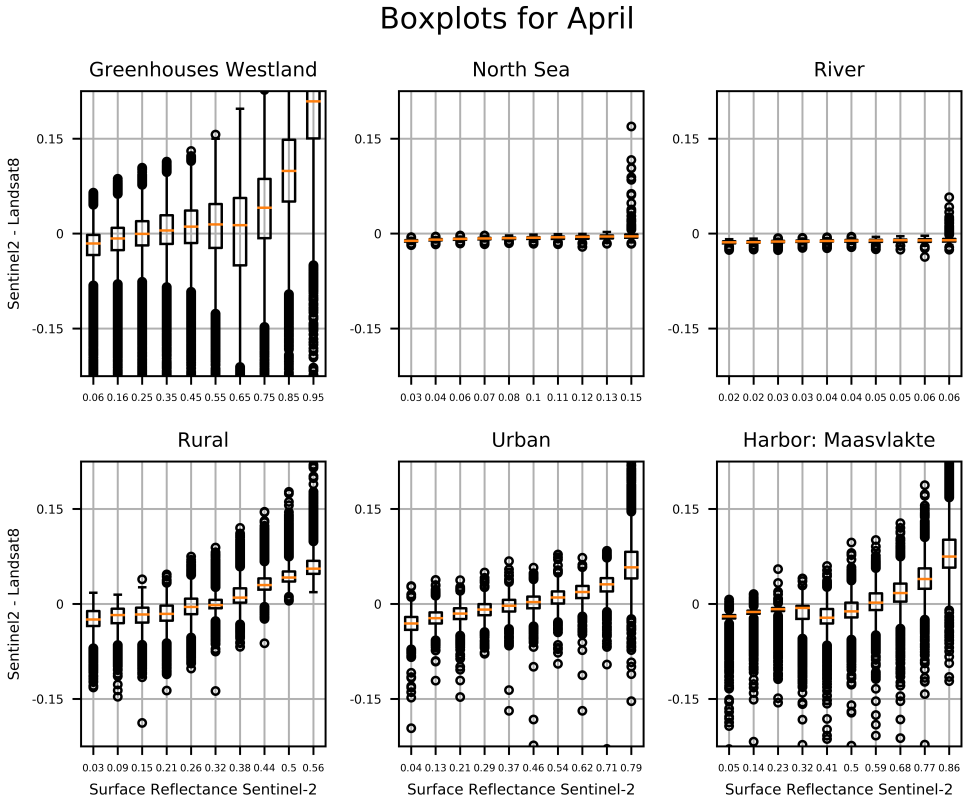

Figure 3.25: Boxplots of absolute differences of all 6 subsets, Landsat-8 subtracted off of Sentinel-2, for the April dataset

The boxplots show the differences of the Sentinel-2 dataset and the Landsat-8 dataset against the surface reflectance of the Sentinel-2 dataset. What stands out immediately are the two water subsets, River and North Sea. These datasets show a very constant boxplot. This can be interpreted as very small differences between the two datasets. The small difference which was concluded by looking at the difference maps and the histograms can be seen by close inspection though. It shows very small negative values, ranging from 0.01 to 0.001, over almost the whole range of surface reflectance values. This shows the consistent higher values of the Landsat-8 surface reflectance pixels. The Rural, Urban and Harbor: Maasvlakte datasets all show negative values for the smaller values of Sentinel-2 and positive values for the higher values. This positive slope of the line connecting all the median values of the boxplots

of absolute differences for these regions is directly related to the fact that the Landsat-8 distributions are more compact/narrow than those of Sentinel-2. The difference is most likely due to the differences in atmospheric correction schemes, i.e. the treatment of the aerosols. The odd one out is again the Greenhouses Westland subset. The boxplots for this subset show very high differences, ranging from 0.05 to 0.21. The same pattern as before can be seen though.

3.4 Surface albedo climatology based on OMI

On July 15$^{\text{th}}$ 2004 NASA launched AURA. One of the instruments on board is the *Ozone Monitoring Instrument*. This instrument makes air quality measurements, e.g. NO_2 & O_3 in the Ultraviolet and Visible parts of the electromagnetic spectrum. OMI provides daily global coverage with a resolution of 13 km x 24 km.

Since the data-series has been (almost) continuous since its launch, a large number of derived products have been created. One of these products is called the OMI LER Albedo Climatology. This dataset is a global albedo dataset with pixel sizes of 0.5°x 0.5°. This dataset is the albedo data used for the, newly launched, TROPOMI products.

The OMI LER Albedo Climatology defines the reflectance at the top of the atmosphere (R) as:

$$R = \frac{\pi * I}{\mu_0 E_0} \tag{3.1}$$

Where:

I : radiance reflected by the Earth
E_0 : incident solar irradiance at TOA perpendicular to the solar beam
μ_0 : cosine of the solar zenith angle

Since the albedo climatology assumes a Lambertian isotropic surface reflectivity (A_s):

$$R(\mu, \mu_0, \phi - \phi_0) = R_0(\mu, \mu_0, \phi - \phi_0) + \frac{A_s t(\mu_0) t(\mu)}{1 - A_s S^{(*)}} \tag{3.2}$$

Where:

μ : cosine of viewing zenith angle θ on the ground
R_0 : the atmospheric reflectance in absence of a surface

By rewriting the previous formula the following formula can be achieved:

$$A_s = \frac{R - R_0}{t(\mu)t(\mu_0) + s^*(R - R_0)} \tag{3.3}$$

Where:

t : function which describes the total atmspheric transmission
s^* : spherical albedo of the atmosphere from illumination from below

This formula is used to find the surface's Lambertian equivalent reflectance (A_s) which corresponds to the observed TOA reflectance [11].

The OMI LER albedo climatology uses an atmospheric correction by using a lookup table created using a radiative transfer model. This method of using this radiative transfer model is more feasible than calculating the atmospheric parameters needed in equation 3.4 with a radiative transfer model for every single measurement. The used radiative transfer model is the *Doubling-Adding KNMI* (DAK) model.

This lookup table contains different atmospheric reflectance values, geometries and other influencing parameters which can occur. By interpolating the measured values for these parameters the corresponding atmospheric reflectance as a function of these measurements can be extracted.

Kleipool et al. do conclude that the different approach which has been taken in the processing of this dataset compared to its predecessors leads to higher surface reflectance compared to the older TOMS and GOME albedo datasets. They also mention that clouds are a significant error source. These conclusions should be taken into account while working with this dataset [11].

This chapter has described the three different surface reflectance/albedo datasets, i.e. Sentinel-2, Landsat-8 and the OMI LER albedo climatology. Also a comparison between Sentinel-2 and Landsat-8 has been done on their high original resolution. The following chapter will compare all three datasets, after they have been put onto the same grid, which is the grid generated by the TROPOMI measurements, by averaging and assigning the correct corresponding values.

4 Surface Reflectance on TROPOMI grid

The previous chapter showed the comparison and differences of the two high resolution datasets used in this research, Landsat-8 and Sentinel-2. The goal of this research is however checking whether the TROPOMI product can be improved by choosing a higher resolution surface reflectance dataset as a-priori data instead of the now used OMI surface reflection product. In order to compare all the used datasets from this research (Landsat-8, Sentinel-2, TROPOMI and OMI) it is imperative that all these datasets are on the same grid and with the same resolution.

This chapter shows all used datasets regridded, interpolated and averaged so all datasets are positioned on exactly the same grid. The grid which is used as the *goal-grid*, so to which the other datasets are regridded, is the grid of the TROPOMI dataset. This grid was chosen since the TROPOMI dataset is the one which this research is focussing on improving. The figure below, figure 4.1, shows the area which this research is focussed on with the grid of the TROPOMI dataset so the sizes and shapes of the TROPOMI pixels become clear.

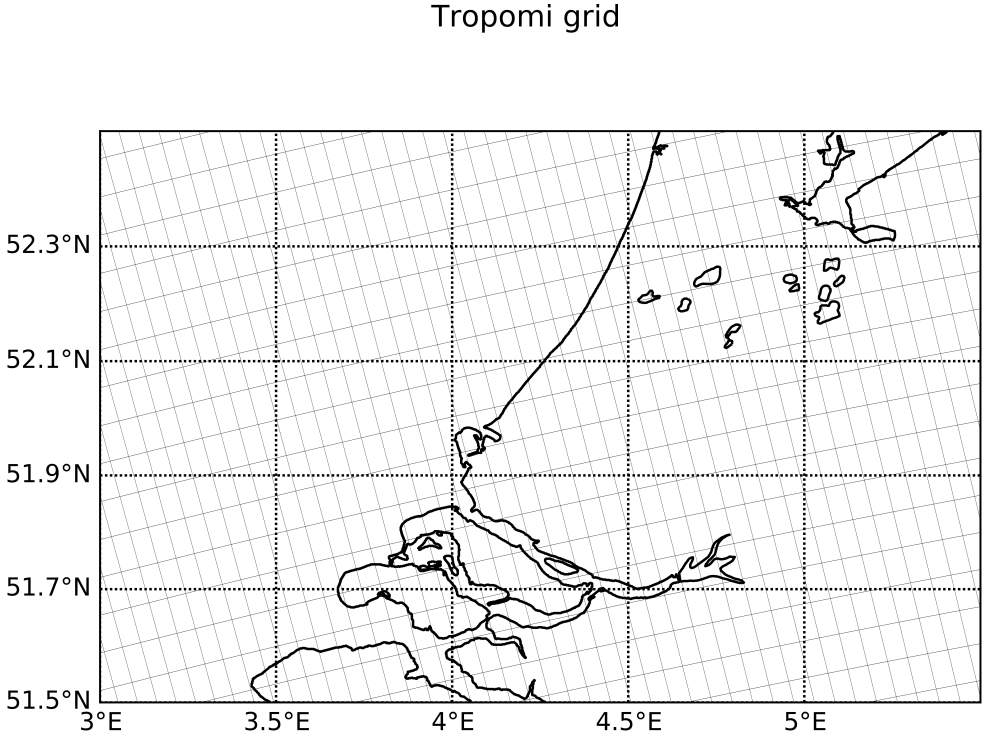

Figure 4.1: The TROPOMI grid for the April dataset

The TROPOMI pixels have dimensions of 7 km x 3.5 km [27]. The a-priori input data of OMI has pixels which are much larger, 13 km x 24 km. Therefore the OMI data has to be manipulated in such a way that is placed directly onto the TROPOMI grid. This is done by determining which TROPOMI pixels lie inside of an OMI pixel and then assigning the corresponding OMI value to all of the included TROPOMI pixels. Below, in figure 4.2, the procedure can be seen in a flow-chart:

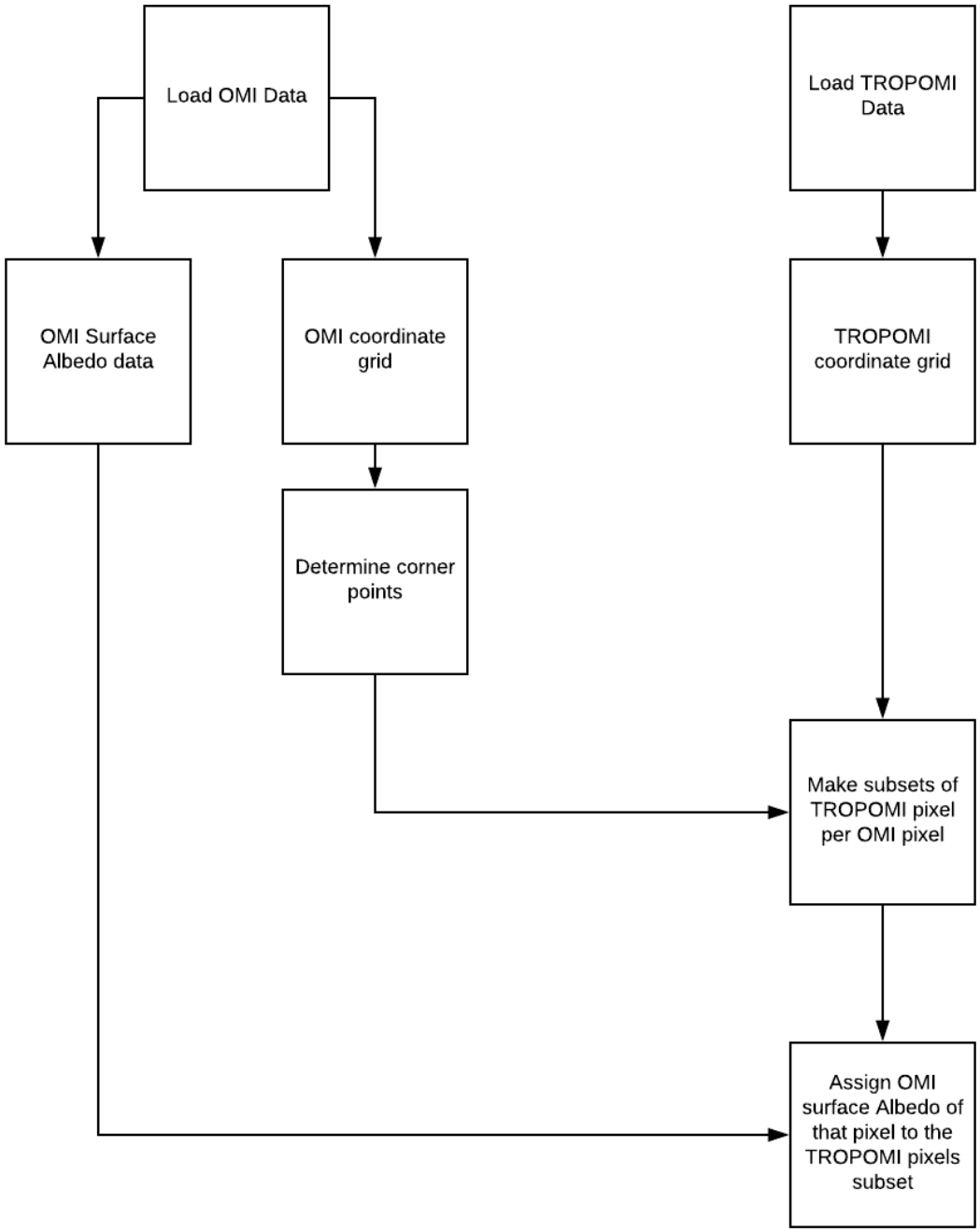

Figure 4.2: Flow chart of the OMI to TROPOMI regridding procedure

When the OMI LER albedo climatology data is placed onto the grid of the TROPOMI pixels, the following figure 4.3 is obtained:

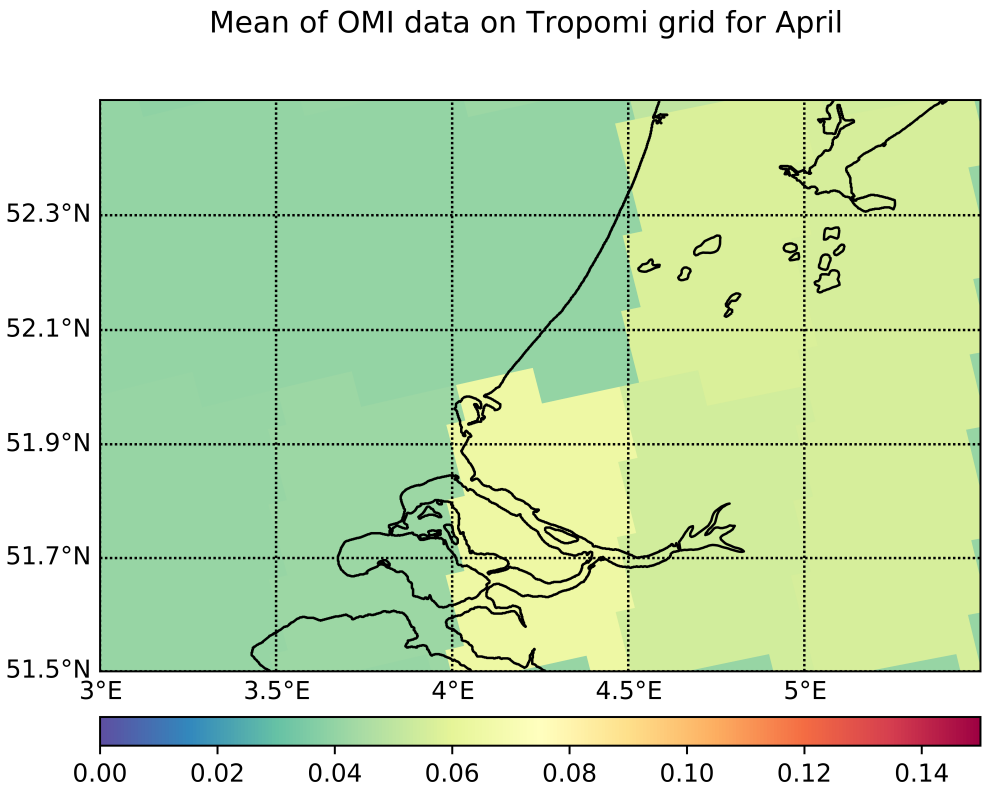

Figure 4.3: The OMI LER albedo data on the TROPOMI grid for the April dataset.

From figure 4.3 it becomes clear instantly that the resolution of the a-priori OMI LER albedo climatology database is not sufficient enough to be of the same level of detail as the TROPOMI data. The figure shows that the available data is spread out over the smaller TROPOMI pixels, due to the lower resolution of the a-priori dataset. The available Sentinel-2 surface reflectance dataset has a much higher resolution. Therefore this dataset can be used to create a surface reflectance dataset with the same resolution as the TROPOMI data. Below the procedure to create this dataset can be seen in a flow-chart in figure 4.4.

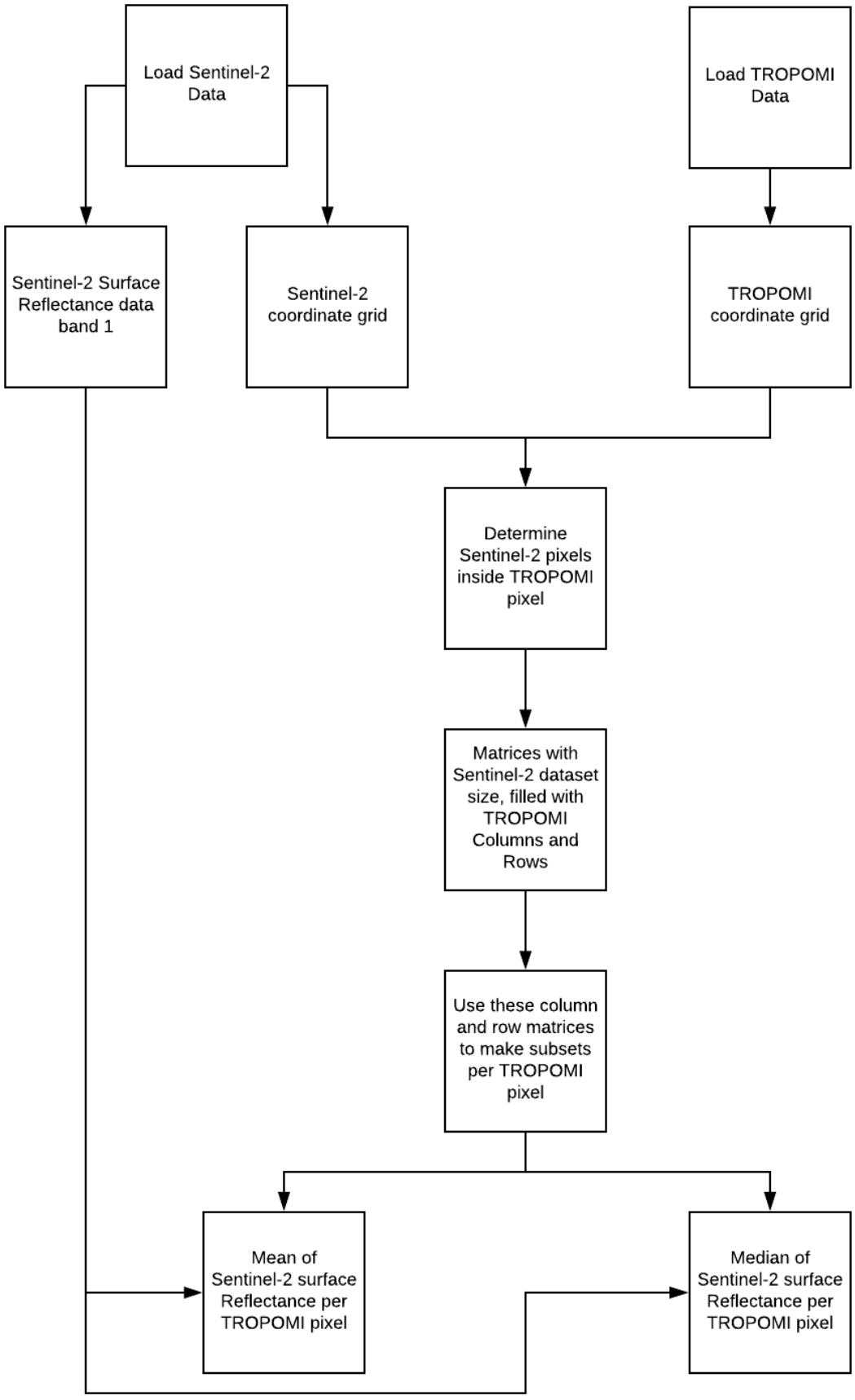

Figure 4.4: Flow chart of the Sentinel-2 to TROPOMI regridding procedure

The following figure, figure 4.5, shows the high resolution Sentinel-2 dataset averaged on the same grid as the TROPOMI dataset. Two methods can be used to assign values to the TROPOMI pixels using the Sentinel-2 data. The mean of the pixels of the high resolution dataset can be taken, but the median of these pixels can also be taken. The median can be seen in the second figure, figure 4.6.

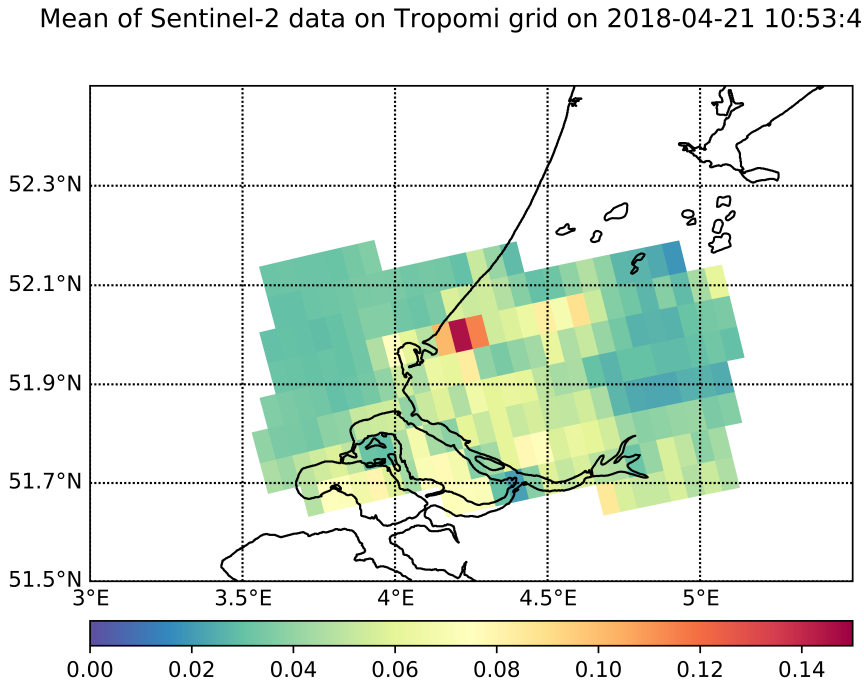

Figure 4.5: The Sentinel-2 surface reflectance data mean on the TROPOMI grid for the April dataset

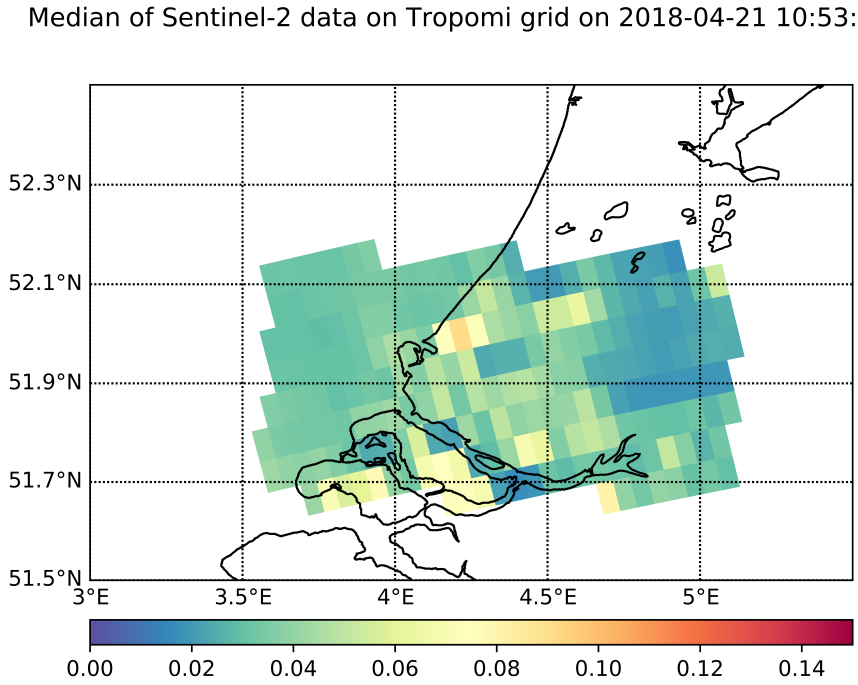

Figure 4.6: The Sentinel-2 surface reflectance data median on the TROPOMI grid for the April dataset

The differences in amount of details between figures 4.5 and 4.6 and the currently used figure 4.3 is instantly clear. Whether the differences these smaller surface reflectance pixels as input data make are significant in comparison with other parts of the process can be visualised by making the same difference plots as in chapter 3. The next figure, figure 4.7, shows the difference between the regridded OMI dataset and the Sentinel-2 dataset averaged onto the TROPOMI grid. First for the April dataset, and the figure after, figure 4.8, shows the difference for the May datasets. It is important to note that the *mean* of the high resolution surface reflectance datasets on the TROPOMI grid is used from now on, not the *median*. This choice was made since the median is used when the outliers are not reliable or their influence on the mean is too large. In this thesis however there are no unreliable outliers, i.e. all data is wanted in the TROPOMI grid version of the high resolution surface reflectance datasets. Also, the TROPOMI resolution is low enough that coincidences which lead to high differences. These coincidences do occur on the resolution of Sentinel-2 and Landsat-8.

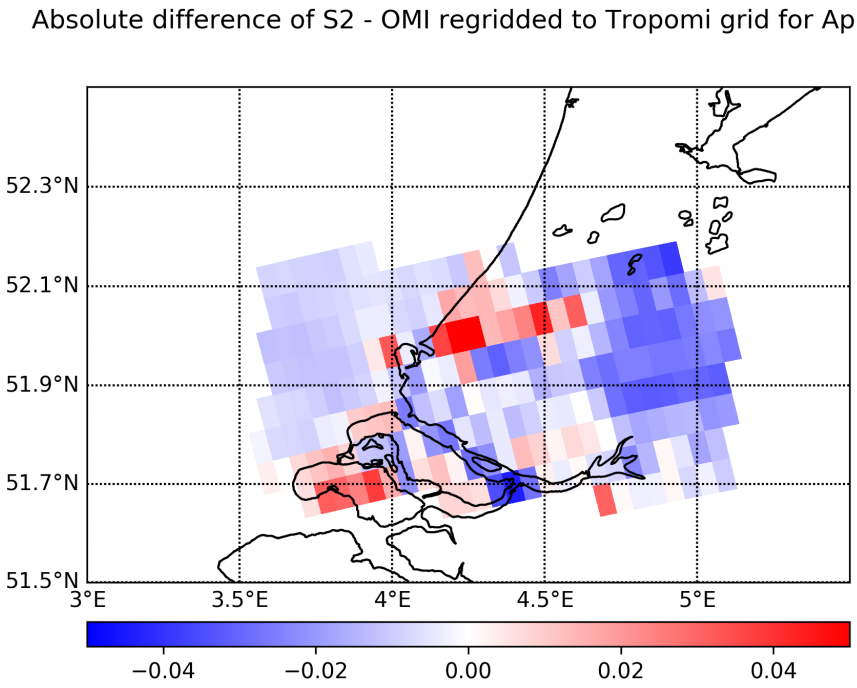

Figure 4.7: OMI surface albedo subtracted off of the Sentinel-2 surface reflectance data mean on the TROPOMI grid for the April dataset

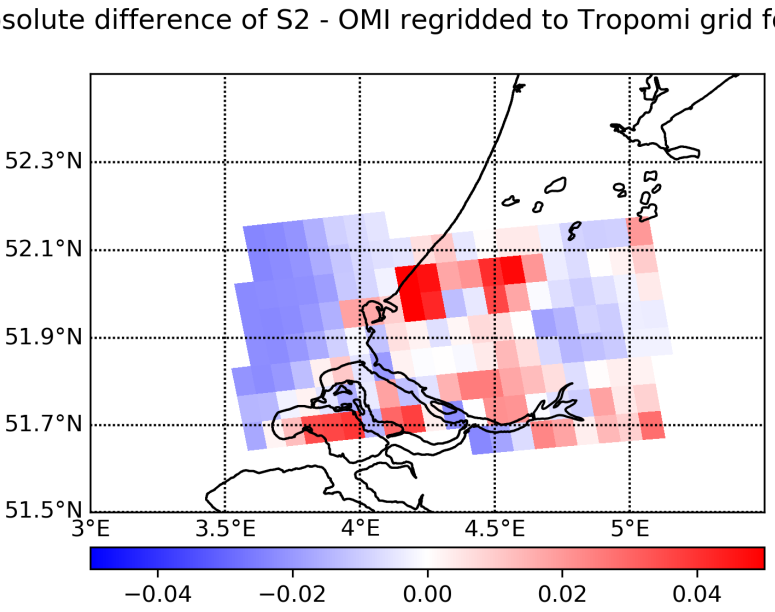

Figure 4.8: OMI surface albedo subtracted off of the Sentinel-2 surface reflectance data mean on the TROPOMI grid for the May dataset

In order to determine whether the differences between the Sentinel-2 and Landsat-8 surface reflectances are significant in comparison to the differences of Sentinel-2 and OMI surface albedo, the same figures can be made for the differences of Landsat-8 and Sentinel-2. The following steps were taken, averaging both Landsat-8 and Sentinel-2 pixels inside an TROPOMI pixel and regridding to the same grid. Figures 4.9 and 4.10 were obtained using this method:

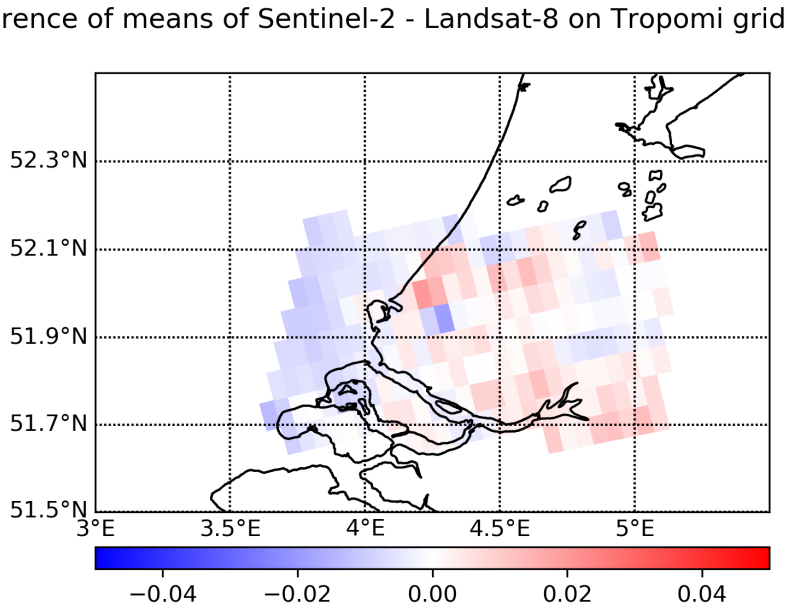

Figure 4.9: Differences of Sentinel-2 and Landsat-8 surface reflectance regridded and averaged to the TROPOMI grid for the April datasets

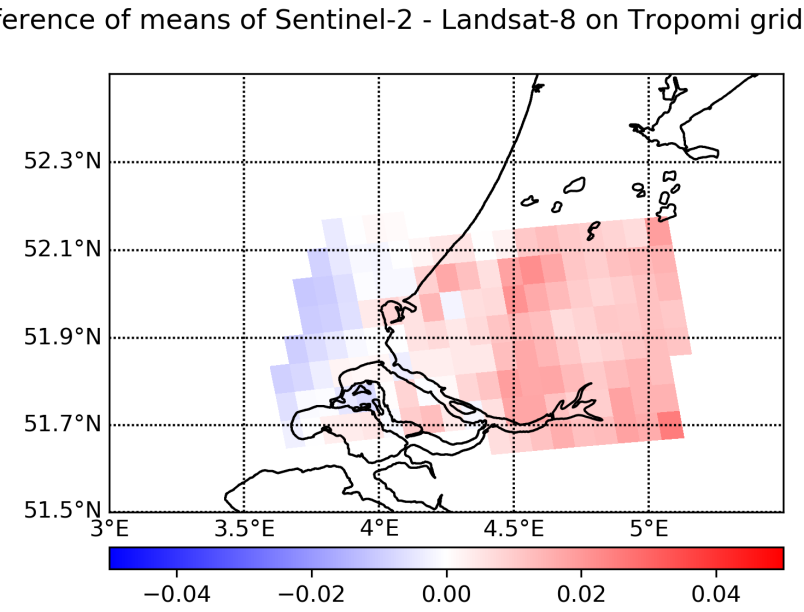

Figure 4.10: Differences of Sentinel-2 and Landsat-8 surface reflectance regridded and averaged to the TROPOMI grid for the May datasets

The figures 4.9 & 4.10 show that differences are still present, and can not entirely be neglected. However, compared to the figures 4.7 and 4.8 the differences are significantly smaller.

In figure 4.10 the clear inconsistency between the Western and Eastern part is visible, as was the case in chapter 3 in figure 3.9. This was to be expected, since the figure shows the same differences, only regridded to a lower resolution. In chapter 3 the cause of this inconsistency was explained by the data delivery of Sentinel-2, which provides data in 'granules' following the UTM projection system, where each of these granules (or tiles) is processed separately to the Level-2 surface reflectance product.

This chapter made comparisons between the currently used albedo dataset, the OMI LER albedo climatology, and the two alternative high resolution surface reflectance datasets. This was done on the resolution and grid of the TROPOMI product. The next chapter will show the calculations and comparisons of different *Air Mass Factors* calculated using the three different surface reflectance/albedo datasets.

5 Impact of the surface reflectance on the air mass factor

In chapter 2 the NO_2 retrieval method was described. One of the components of this retrieval method was the so-called *Air Mass Factor* (AMF). This value is the link which connects the Slant column and the vertical column in the following manner:

$$N^V = \frac{N^S}{AMF} \tag{5.1}$$

It is important to note that the vertical column density, so the amount of an atmospheric component, is inversely related to the AMF. Therefore, a higher AMF value corresponds with a lower vertical column density.

Formula 5.1 looks simple, however it is a challenge to obtain the correct value for the Air Mass Factor. One way of doing this is by using the *Lambert-Beer* law, as explained in the second chapter [28]:

$$I(\lambda) = I_0(\lambda) * e^{(-\tau_s)} \tag{5.2}$$

In formula 5.2, $I(\lambda)$ denotes the measured radiance, $I_0(\lambda)$ is the irradiance and τ_s is the total slant optical depth. The variable τ_v can be interpreted as the value which links the direct solar radiation to the measured radiation. It is also dependent on the path length through the concerned atmospheric component. This value is the sum of different components:

$$\tau_s = \tau_s^{aerosols} + \tau_s^{Rayleigh} + \tau_v^{NO_2} * AMF^{NO_2} + \tau_v^{O_3} * AMF^{O_3} + ... \tag{5.3}$$

Formula 5.3 shows that the slant optical depth, τ_s, of an atmospheric component is equal to the vertical optical depth of that component times its Air Mass Factor, here denoted as AMF. Therefore the wanted vertical optical depth can be calculated from measurements when this AMF is known.

In the wavelength regime focussed on in this research, the UV-VIS regime, the two slant components, $\tau_s^{Aerosols}$ & $\tau_s^{Rayleigh}$, are the dominant factors. The Rayleigh factor is, however, very well defined, and thus they can be corrected for. The Aerosol factor is not so well defined, but this has a smooth wavelength dependency. [29]. In the case of simulations these corrections are not necessary since the influence is already known.

The following step taken in this research was creating a *Look-up table* (LUT) from which the AMF values for the pixels of the case studies could be derived. A *Radiative Transfer Model* (RTM) was needed to create this LUT. A radiative transfer model describes the propagation of electromagnetic radiation through a medium, in this case the Earth's atmosphere. The LUT of this research was created using the *Doubling Adding KNMI* (DAK) radiative transfer model [30].

Contrary to the physical measurements made by the satellites, the vertical columns of all the different atmospheric components are known in a model. This leads to the option of using the model to calculate the AMF values, which can later be used to determine the vertical columns with the actual satellite measurements. The *Radiative Transfer Model* (RTM), in this case the DAK model, calculates, among others, the *Top Of Atmosphere* (TOA) radiation for given: wavelength, atmospheric composition, the solar and viewing zenith angles and the surface characteristics (often the albedo). The atmospheric composition also includes the vertical profiles of the pressure and temperature, the aerosol extinction and the trace gases.

The slant column can be calculated in different ways. One way is to use the RTM to calculate the radiance spectrum, which is a simulated satellite measurement, and then applying the DOAS method in order to calculate the slant column. The problem with this approach is the fact that this takes a lot of computational power since it has to be done for every wavelength. Another way of doing this is by making simulations at one particular wavelength. This is also the approach used for this research, due to its smaller computational load.

This approach leads to the possibility of using the formula below:

$$I^{NO_2^{+10\%}} = I^{NO_2^{Reference}} * e^{-AMF^{NO_2} * \Delta\tau^{NO_2}} \tag{5.4}$$

$$\text{With: } \Delta\tau^{NO_2} = \tau^{NO_2^{+10\%}} - \tau^{NO_2^{Reference}} \tag{5.5}$$

Formula 5.5 shows a perturbation of 10% being used. This value can also be altered, since it doesn't influence the required AMF value for the optically thin regime. Since all the parameters in this formula, except the AMF, are known, the AMF can be calculated. Rewriting leads to:

$$AMF = \frac{\ln(I^{NO_2^{Standard}}) - \ln(I^{NO_2^{+10\%}})}{\tau^{NO_2^{+10\%}} - \tau^{NO_2^{Standard}}} \tag{5.6}$$

If the perturbation is done only in a thin layer at height z, then this formula can be used to obtain the altitude resolved AMF. The LUT provides the values for $I^{NO_2^{Standard}}$, $\ln(I^{NO_2^{+10\%}}$, $\tau^{NO_2^{+10\%}}$ & $\tau^{NO_2^{Standard}}$, which are needed in formula 5.6. These values are obtained by providing the following parameters: *Solar Zenith Angle* (SZA), *Viewing Zenith Angle* (VZA), *Relative Azimuth* (relAZIM), *Aerosol Optical Depth* (AOT), *Top Height of Aerosol layer* (PBL), *Surface Reflectance* (SR) & the heights at which the AMF needs to be known. These AMF values which are valid for a certain 'slice' of the atmosphere are named *box-AMFs*. Figure 5.1 shows different box-AMF values for differing surface reflectances and heights. These box-AMF values were calculated using the DAK radiative transfer model.

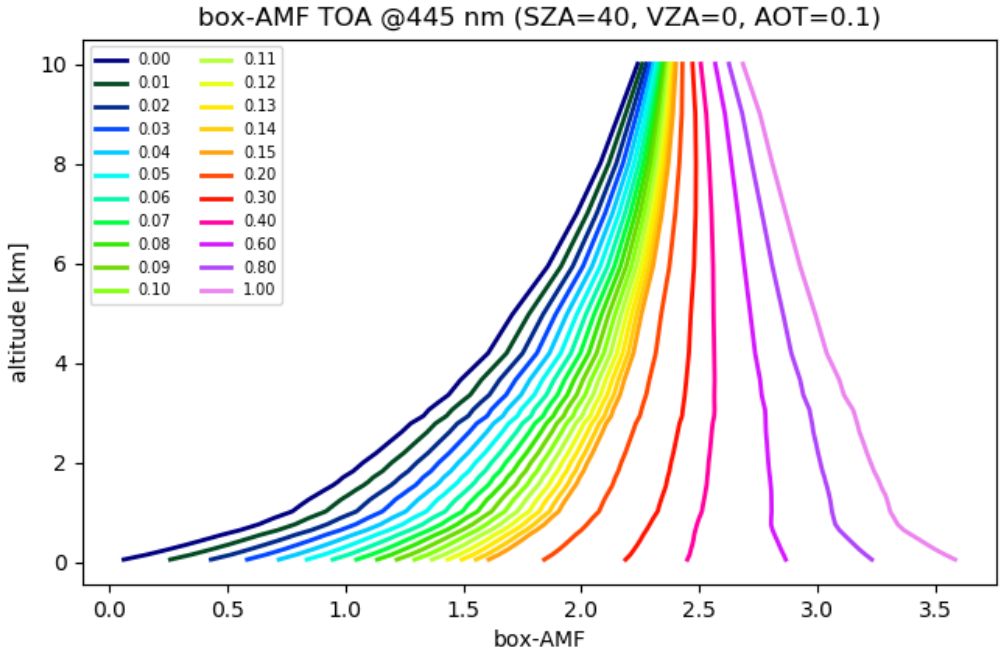

Figure 5.1: Box-AMFs at different altitudes for different surface reflectances. Simulations performes with the DAK radiative transfer model.

The AMF values for the pixels in the TROPOMI grid were calculated by taking the box-AMF values and integrating these over the height. Box-AMF values can be interpreted as a sensitivity and the profile shape is needed in order to determine the weighted mean sensitivity. The following formula was used:

$$AMF = \frac{\int m(z) * n(z) dz}{\int n(z) dz} \tag{5.7}$$

In formula 5.7 m(z) is the box-AMF and n(z) is the profile shape. This research used two block profiles, one with a top height of 400 metres and the other had a top height of 800 metres.

All input values were obtained from the TROPOMI dataset, with one important distinction: in one outcome the currently used OMI surface albedo value was used as Surface Reflectance value, while in the other outcomes the two high resolution surface reflectance datasets were used (regridded and averaged to the TROPOMI grid): Sentinel-2 and Landsat-8.

Multi-dimensional linear interpolation was used to obtain the box-AMF for any value of SZA, VZA, surface reflectance and AOT.

5.1 Current albedo input dataset

In this section the calculated Air Mass Factors using the OMI LER albedo climatology are shown. This dataset is currently used as a-priori in the Level-2 processing for the TROPOMI NO_2 product.

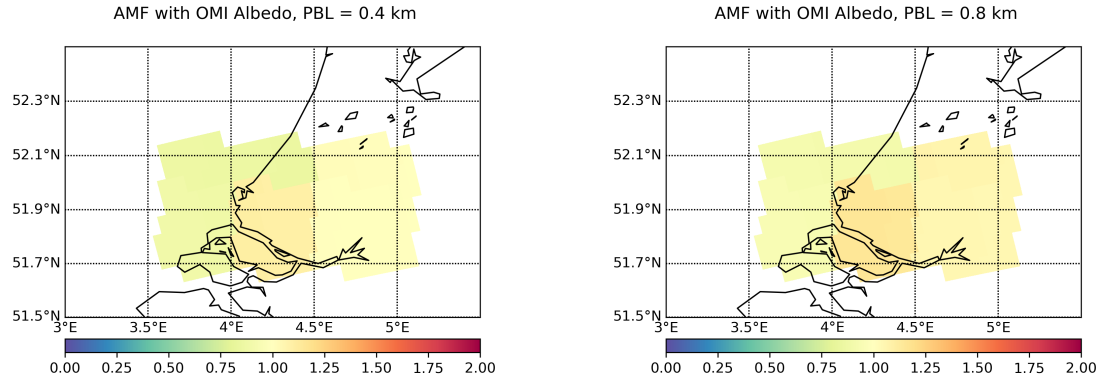

Figure 5.2: Air Mass Factor values for block profiles with a top height of 400 metres (left) & a top height of 800 metres (right) calculated using the OMI albedo dataset for April as input.

Figure 5.2 shows the AMF calculated using the interpolation of the Look Up Table created by the DAK simulation. The input data was all derived from TROPOMI, for example the Solar Zenith Angle of that overpass, except for the surface reflectance input. This originated from the OMI LER albedo climatology dataset. The figures show the results for the 21st of April. The following figures, figure 5.3, show the outcomes for the May dataset.

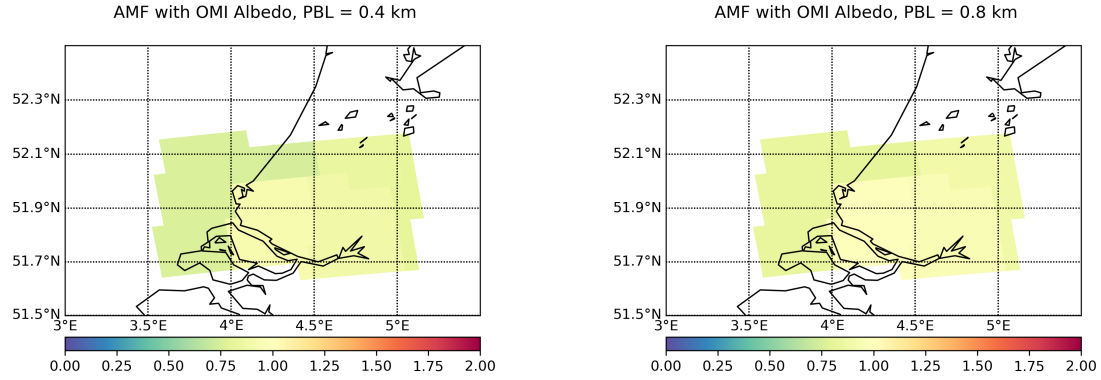

Figure 5.3: Air Mass Factor values for block profiles with a top height of 400 metres (left) & a top height of 800 metres (right) calculated using the OMI albedo dataset for May as input.

When figure 5.2 is compared to figures 4.3 it can be seen that the data in both figures follows the same pattern, illustrating the fact that on this spatial scale, spatial gradients in the AMF are mostly due to gradients in the surface reflectance. When the OMI LER climatology is used as input for the Air Mass Factor calculations very little spatial variability can be seen. When the Sentinel-2 dataset is used the spatial variability, the pixel-to-pixel variations, are higher, as well as a wider range in the AMF values.

Furthermore, the figures show AMFs for the two profile shapes used in all the simulations, box profiles from the surface to 400 and 800 metres top-height respectively. Since the outcomes of the simulations were very similar for the two heights (small differences of 0.03 to 0.07 are present), and the surface reflectance proved to have a much higher influence on the AMF value, only the 800 metre profile top height outcomes are shown from here onwards.

5.2 Alternative high resolution surface reflectance input datasets: Sentinel-2 & Landsat-8

The following section will show the AMF outcomes using the two high resolution surface reflectance datasets, Sentinel-2 and Landsat-8. The first dataset shown is Sentinel-2 and following Landsat-8's outcomes will be shown.

The following figures, 5.4 & 5.5, show the Air Mass Factors for the Greater Rotterdam area using the regridded surface reflectance values of Sentinel-2 as input, for the April and May datasets.

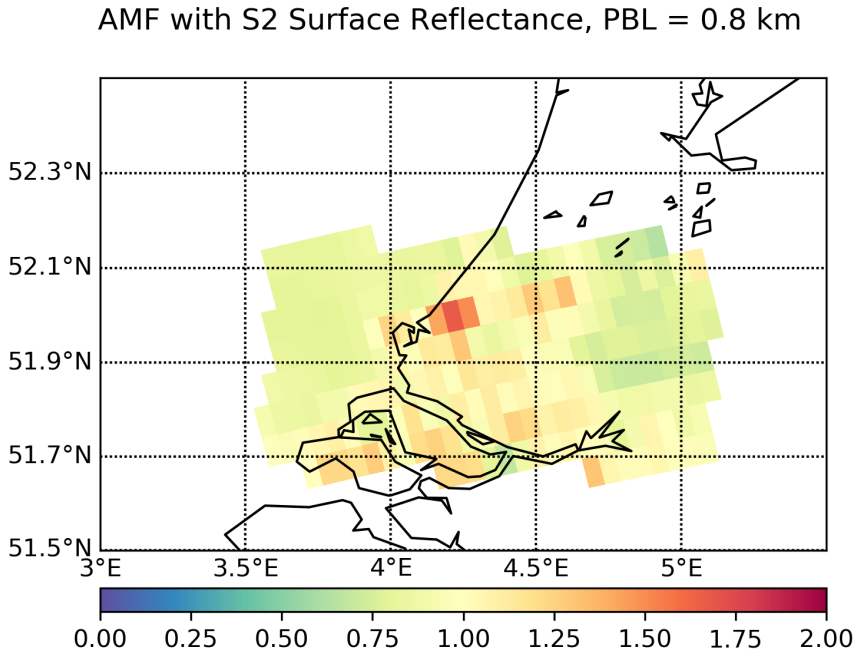

Figure 5.4: Air Mass Factor values for block profiles with a top height of 800 metres calculated using the Sentinel-2 surface reflectance dataset for the 21st of April as input.

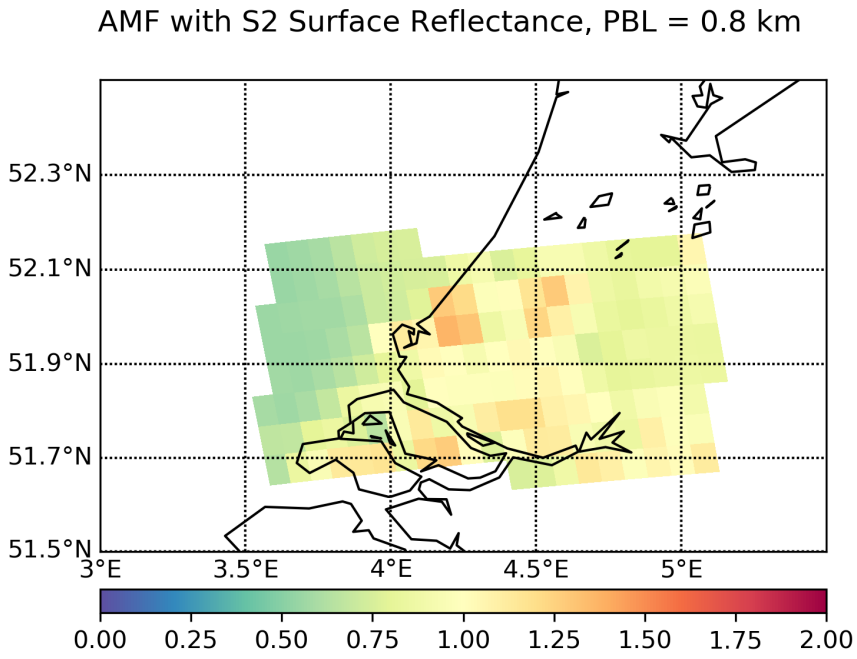

Figure 5.5: Air Mass Factor values for block profiles with a top height of 800 metres calculated using the Sentinel-2 surface reflectance dataset for the 6th of May as input.

When these figures are compared to the figures of the AMF values created using the OMI LER albedo climatology as input, figure 5.2 & 5.3, the differences become clear immediately. The high resolution surface reflectance input leads to a higher spatial variability. The 'Westland' region can be clearly distinguished again, as was the case in the surface reflectance figures in chapter 3. This is especially the case for the April dataset. Note that differences in extreme values between April & May, again mostly in the Westland region, are partly due to the fact that the precise location of the TROPOMI pixels is different. This may lead to smoothing of hot-spots in the surface reflectance.

The following figures, 5.6 & 5.7, show the AMF values for the Greater Rotterdam area using the Landsat-8 surface reflectance values as input, for the April and May datasets.

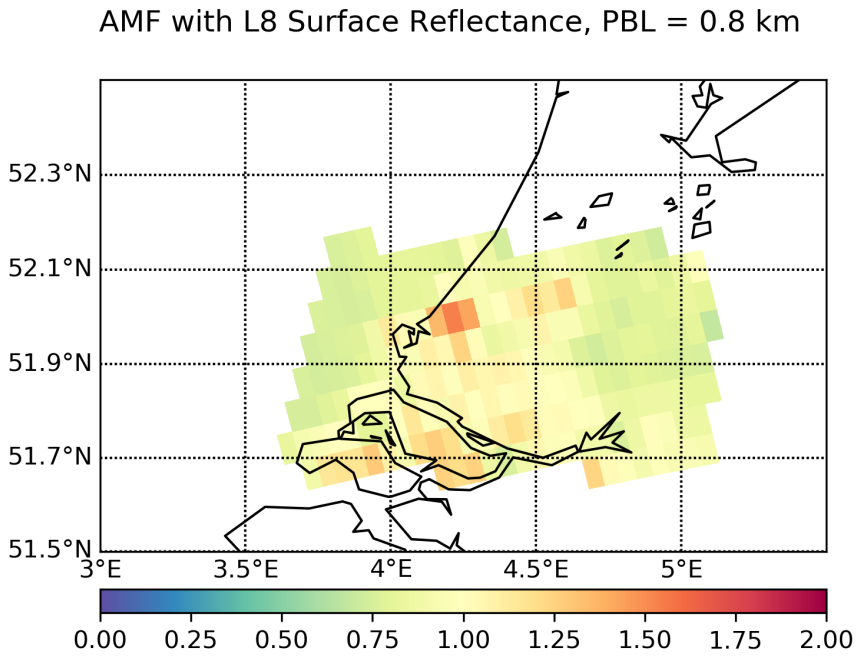

Figure 5.6: Air Mass Factor values for block profiles with a top height of 800 metres calculated using the Landsat-8 surface reflectance dataset for the 21st of April as input.

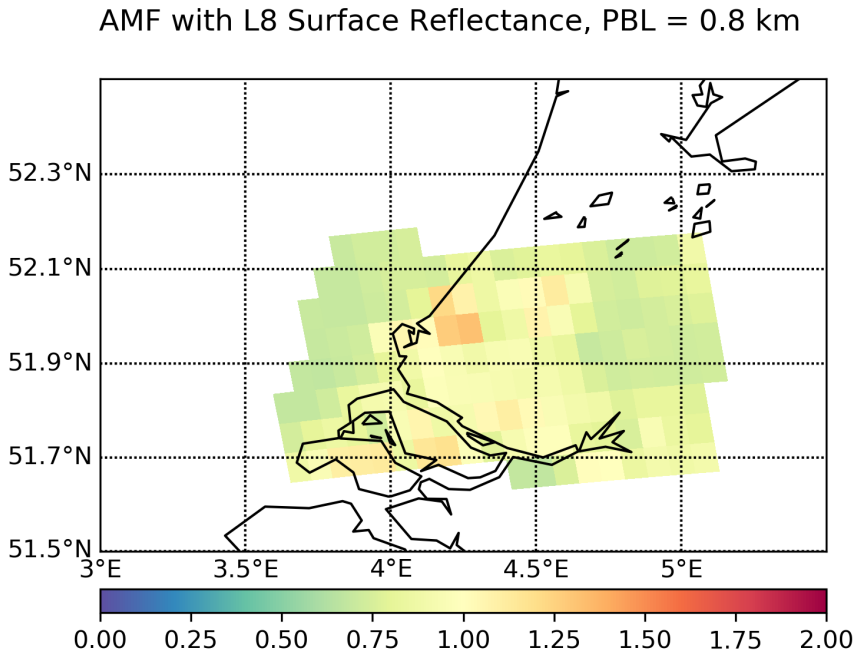

Figure 5.7: Air Mass Factor values for block profiles with a top height of 800 metres calculated using the Landsat-8 surface reflectance dataset for the 6th of May as input.

The maps depicting the AMF values created using the surface reflectance values of Landsat-8 show comparable results to the maps created by using the surface reflectance data of Sentinel-2. The same patterns can be observed with comparable 'hot-spots'. The differences with the AMF values using the OMI albedo dataset become clear instantly.

5.3 Analysis of differences

The next step taken, and main objective of this study, was calculating the differences between the different AMFs, i.e. the two high resolution surface reflectance AMF values and the currently used OMI LER albedo climatology. This was done in roughly the same way as in the previous chapter.

The relative difference was calculated as follows:

$$\frac{(A-B)}{A} * 100\% \tag{5.8}$$

Where A & B can be either the AMF values calculated using the Sentinel-2, Landsat-8 or OMI surface reflectance input values. For this research the following differences were calculated and these will also be shown in the following sections: the relative difference between Sentinel-2 and OMI's AMFs (which can be seen in figures 5.8 & 5.9) and the differences between Sentinel-2 and Landsat-8's AMFs (which can be seen in figure 5.10 & 5.11). In both cases the Sentinel-2 surface reflectance is used as reference.

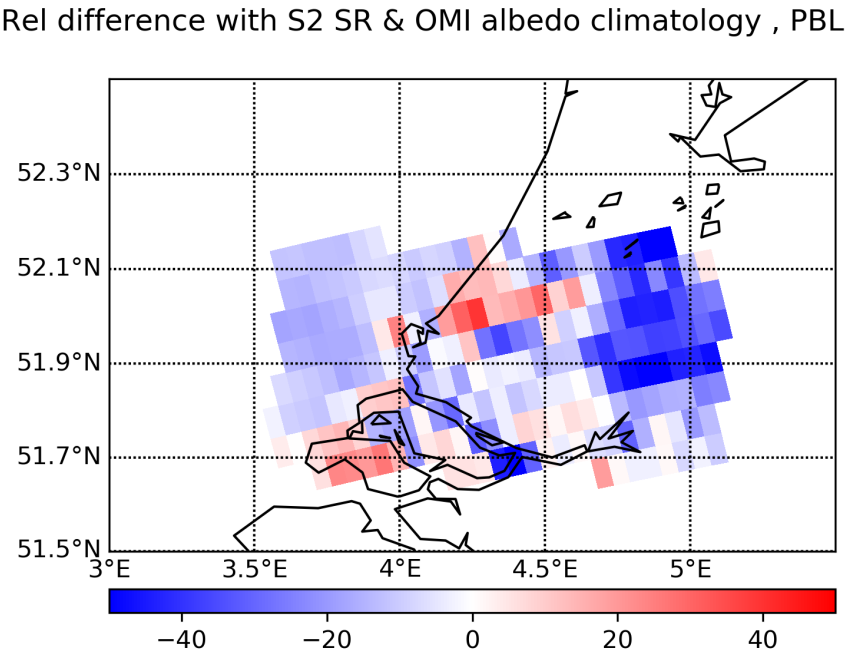

Figure 5.8: The relative differences between the Air Mass Factor values for block profiles with a top height of 800 metres calculated using the Sentinel-2 & OMI surface reflectance datasets for the 21st of April as input.

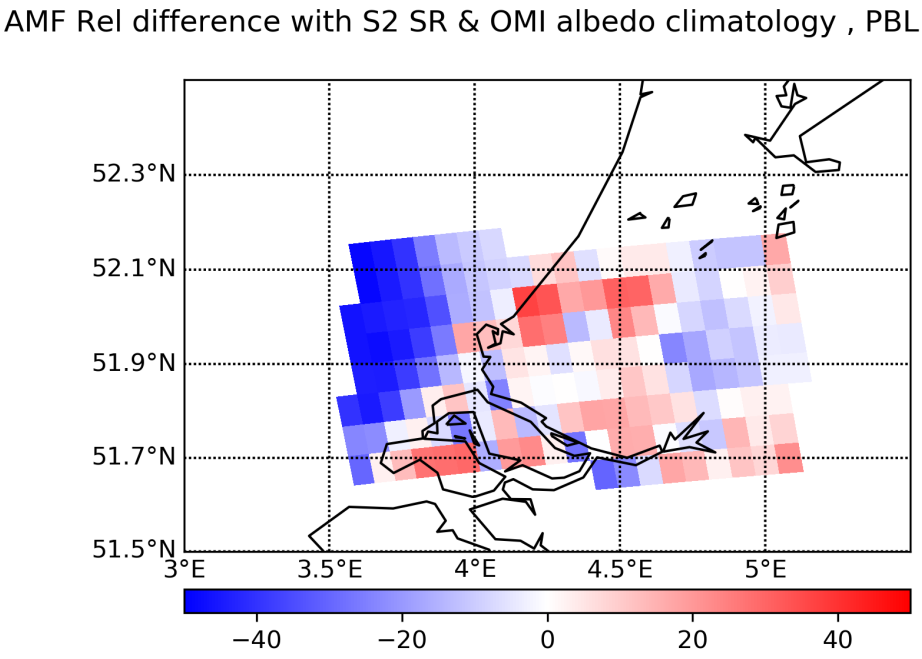

Figure 5.9: The relative differences between the Air Mass Factor values for block profiles with a top height of 800 metres calculated using the Sentinel-2 & OMI surface reflectance datasets for the 6th of May as input.

These figures show that the accuracy of the AMFs of regions with a high surface reflectance is strongly dependent on spatial resolution, whereas the accuracy in regions with low surface reflectance mostly depends on the effectiveness of the atmospheric correction scheme. This is due to the fact that for low values, small differences in the surface reflectance value lead to a relatively big effect in the AMF, while at higher values these differences lead to smaller effects in the AMF. This effect can be seen in figure 5.1.

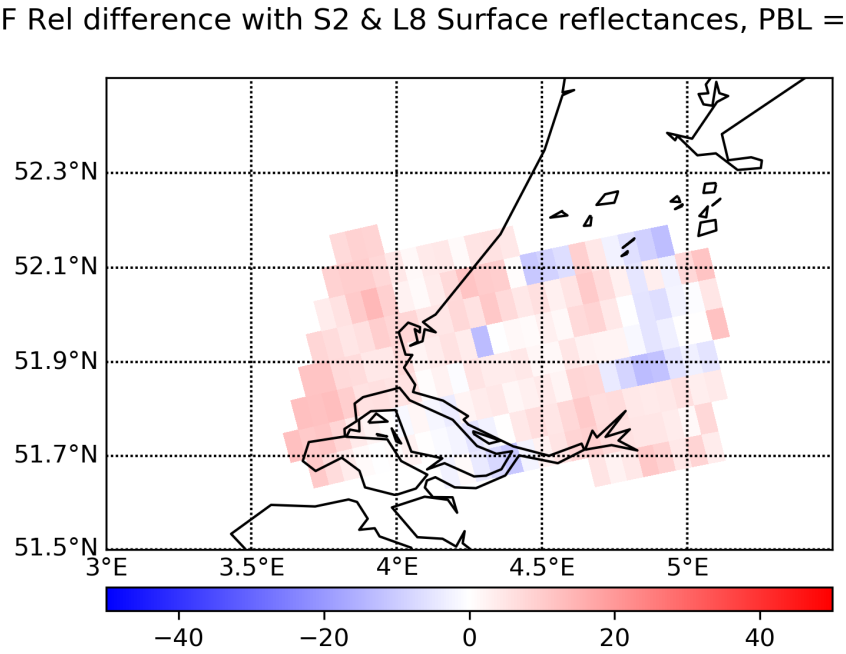

Figure 5.10: The relative differences between the Air Mass Factor values for block profiles with a top height of 800 metres calculated using the Sentinel-2 & Landsat-8 surface reflectance datasets for the 21st of April as input.

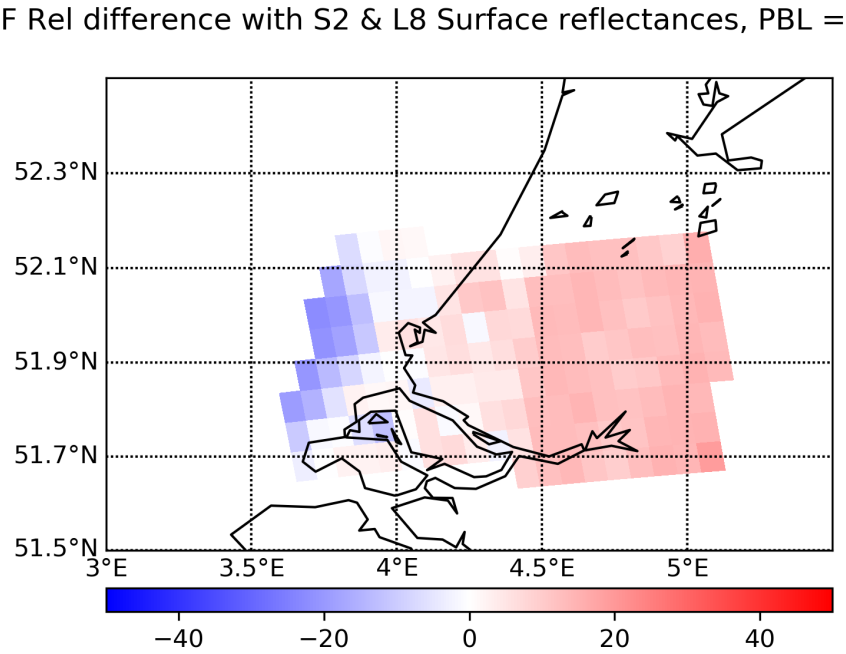

Figure 5.11: The relative differences between the Air Mass Factor values for block profiles with a top height of 800 metres calculated using the Sentinel-2 & Landsat-8 surface reflectance datasets for the 6th & 7th of May as input.

These difference maps show clearly that the differences between Sentinel-2's surface reflectance AMFs and the AMFs created using the currently used OMI LER albedo climatology have significantly larger differences compared to the AMFs created using the two high resolution surface reflectance

datasets. This is important because this implies that, despite differences between Sentinel-2 & Landsat-8, the currently used a-priori surface albedo data should be improved in order to match the high resolution of the TROPOMI observations.

An interesting feature in figure 5.11 is the substantial positive bias (≈10%) in the entire eastern part of the map. This can be explained the same way as for figure 3.9, where it became clear that the Sentinel-2 data acquisition used different granules to 'stitch' an image together. The eastern part therefore has a different acquisition time, which explains the consistently different and higher AMF values, since a different acquisition time leads to different solar and viewing zenith angles as well as other characteristics.

Apart from maps to visualise the differences, statistics can also be utilised. In order to make these statistical comparisons the difference datasets of April and May were combined. The AMF values calculated using the two different top-heights for the block shaped profiles, 400 and 800 metres, were both calculated. Since a top height of 800 metres is more common to use and since the outcomes were in agreement with each other, only the 80 metre top height outcomes are shown. The first step in making the statistical comparison was to create the histograms of the relative differences (figure 5.12).

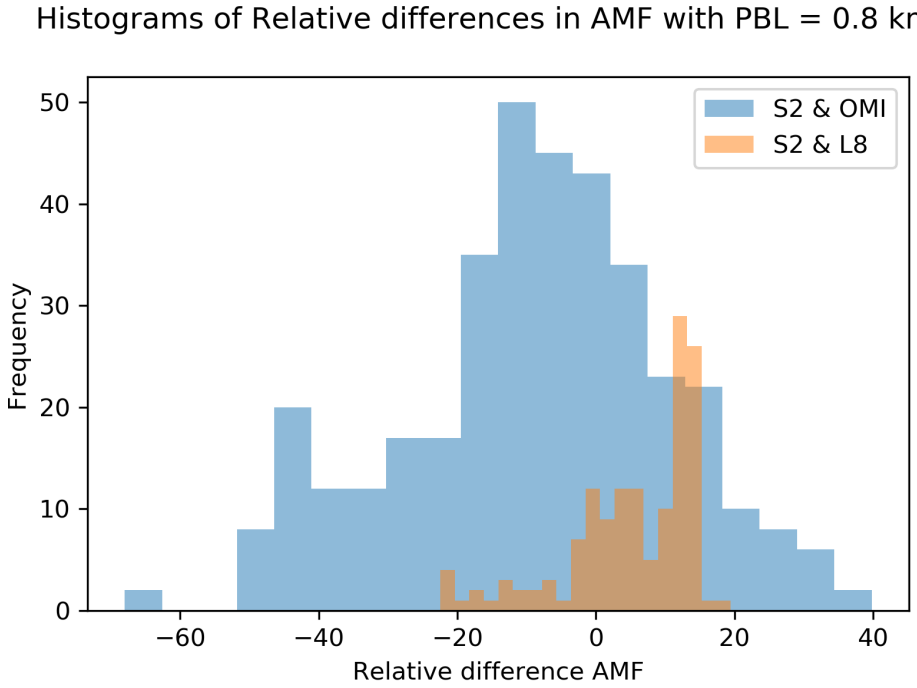

Figure 5.12: The histogram of the relative differences between the OMI, Sentinel-2 & Landsat-8 datasets. The data for the profile top height of 800 metres. Both the datasets of April and May were combined for this figure.

The histogram reveals that the relative AMF differences between Sentinel-2 and the OMI LER albedo climatology show a large spread and quite big differences. The high-resolution datasets AMFs, Sentinel-2 and Landsat-8, show smaller differences. It is also clear that more positive relative differences are present, especially around 15%. This means a higher AMF value for Sentinel-2. The differences are however significantly smaller than the difference values for Sentinel-2 and the OMI albedo dataset. That systematic differences seen between Landsat-8 & Sentinel-2 are mostly related to the differences in the atmospheric correction schemes i.e. the treatment of aerosols, as discussed in chapter 3. For differences between the OMI LER albedo database based AMFs and Sentinel-2 based AMFs, both differences in spatial resolution and atmospheric correction schemes are responsible. These findings are supported by the following table 5.1, which shows the differences' ranges and their medians:

April		**min**	**median**	**max**
	(S2-OMI)/S2 * 100%	-68.0%	-10.4%	39.8%
	(L8-OMI)/L8* 100%	-53.9%	-15.6%	36.3%
	(S2-L8)/S2*100%	-13.2%	4.3%	14.0%
May				
	(S2-OMI)/S2 * 100%	-48.6%	-3.9%	37%
	(L8-OMI)/L8* 100%	-43.4%	-9.3%	33.5%
	(S2-L8)/S2*100%	-22.5%	7.2%	19.5%

Table 5.1: Differences of AMFs calculated using the three different surface reflectance/albedo satasets as input.

5.4 Comparison with Ground-based Observations

In 2018a first systematic validation of Sentinel-5p was performed in the framework of a project called: NIDFORVal (S5P NItrogen Dioxide and FORmaldehyde VALidation using NDACC and complementary FTIR and UV-Vis DOAS ground-based remote sensing data) [31]. A part of this research was comparing the TROPOMI NO_2 product with ground-based measurements. This was done for several locations worldwide, of which one was *Cabauw* in the Netherlands. This location is also located in the region investigated in this study, i.e. to the East of the Greater Rotterdam area, and therefore the outcomes of this validation can be compared to this research's outcomes. It is important to keep in mind that only the April outcomes can be compared to this validation since the Cabauw tower is situated in the eastern area of our project which showed the consistent offset due to the 'stitching' done on the Sentinel-2 dataset. The paper showed a mean bias of approximately -25% for the Cabauw location for the NO_2 product, where the bias is calculated as follows:

$$\frac{(SAT - GB)}{GB} * 100\% \tag{5.9}$$

In this formula SAT refers to the satellite, in this case the TROPOMI NO_2 product while GB stands for ground-based, so the NO_2 value measured at the Cabauw location. The outcomes for April are summarised in the following table 5.2:

	Relative difference
(S2-OMI)/S2 * 100%	-34.38%
(L8-OMI)/L8 * 100%	-31.61%
(S2-L8)/S2 * 100%	-2.11%

Table 5.2: Differences of AMFs calculated using the three different surface reflectance/albedo satasets as input, for the Cabauw location.

This difference of approximately -25% is similar in magnitude to the surface reflectance induced bias found in this study, see table 5.2. Further research is needed (i.e. more days and more locations should be included) to confirm this apparent relation.

It is important to note that these values show the AMF value, not the NO_2 product differences. The AMF value and this NO_2 product are inversely proportionate, in other words a higher AMF value leads to a lower NO_2 value and vice versa. Another important detail is the fact that the value used in this research has a flipped sign compared to the project of the Sentinel-5p validation team due to the difference in the nominators in both formulae. In other words; in equation 5.8 the paper used the higher resolution ground-based observation dataset as the B value while this thesis uses the higher resolution Sentinel-2 dataset as the A value.

The outcome of the project by the Sentinel-5p validation team of a underestimation of the NO_2 tropospheric vertical column are in agreement with the outcome of this research, which show that due to the currently used surface albedo input data the AMF values are overestimated, which lead to a lower NO_2 value.

5.5 Discussion

The conclusions drawn from the outcomes derived at in this research should be considered in the framework of this thesis. The results are based on only two case studies, which were not perfect conditions. While the results seem to correlate with the NIDFORVal project, this limited number of case studies is not enough for a definitive comparison. Apart from the limitation from the small number of available cases-studies, the *May* dataset also had the limitation of the Landsat-8 dataset being taken from another day. These high resolution datasets also consisted of surface reflectance data, not albedo data, which creates the problems correlated with the solar zenith angle, viewing zenith angles and other corresponding characteristics. Furthermore, the profile shapes used for the Air Mass Factor calculations were very simplistic and therefore can be considered to be a limiting factor in this thesis.

Future studies should therefore look at the possibilities of obtaining a high resolution albedo dataset. Another possibility is including a large number of days as case-studies, given the fact that as time progresses more of these suitable days will be available. A more realistic and higher resolution profile dataset can also lead to more realistic results.

6 Conclusion & Recommendation

In 2017 the Sentinel-5p satellite was launched by ESA as a precursor to the Sentinel-5 satellite with the main objective to monitor atmospheric components such as: NO_2, O_3, SO_2, $HCHO$. Other characteristics of the atmosphere which will also be measured include the cloud fraction & height as well as the aerosol index & height. Aerosol optical depth is not a product. One of the instruments on board of the Sentinel-5p satellite is the Tropospheric Monitoring Instrument (TROPOMI). This instrument is the successor to the Ozone Measuring Instrument (OMI), launched by NASA in 2004.

One of the main products of TROPOMI is the tropospheric NO_2 product. The retrieval of this product consists of two steps. The first step is the application of the Differential Optical Absorption Spectroscopy (DOAS) method. This spectral analysis technique yields the NO_2 absorption along the average light path. The second step is to derive the appropriate Air Mass Factor (AMF) to convert the slant NO_2 column density, measured by the instrument, to the vertical NO_2 density column. The AMF can be calculated using different parameters and these are partly obtained from the information from the measurements, and partly from external sources (a-priori information).

Currently the accuracy of the a-priori information is one of the main error sources, often leading to systematic biases. The vertical profile shape, currently provided by the TM5 model, which is a global chemistry-transport-model, is one of the a-priori datasets that has quite a large uncertainty. Another a-priori dataset which, for various reasons, often contributes significantly to the total systematic bias is the albedo climatology. The currently used albedo dataset has a much coarser resolution than the TROPOMI pixel sizes. The albedo climatology has pixels of 0.5°x 0.5°, which is roughly equal to 55 km x 34 km at mid-latitudes. The TROPOMI product has a resolution of 3.5 km x 7 km. This leads to the fact that the TROPOMI product does not resolve spatial gradients sufficiently in this parameter. Furthermore, it may be biased due to a residual atmospheric signal, as discussed in chapter 3.

In order to determine if an improvement can be made for the TROPOMI tropospheric NO_2 product, this research investigated the impact of using an alternative, high spatial resolution, surface reflectance dataset instead of the currently used coarse resolution OMI LER albedo climatology. This is investigated for a relatively small spatial region, which is important in the Netherlands because of its high population density and pollution levels: the Greater Rotterdam Area. For this research a surface reflectance (SR) product from the Sentinel-2 satellite is used. This product has resolutions ranging from 10 x 10 metres to 60 x 60 metres (depending on the band) and can be obtained with every cloud free overpass. The first part of this research consisted of comparing this Sentinel-2 surface reflectance dataset to another surface reflectance dataset. The second dataset chosen was the *Landsat-8* surface reflectance dataset, since it is highly renowned. An important first step in this study was to compare the surface reflectance products from these two datasets. Therefore, the Landsat-8 dataset was regridded onto the Sentinel-2 grid. This was done since the pixel centers where somewhat displaced. After this regridding the datasets could be compared on a pixel-by-pixel level.

Observed differences were relatively small, but consistent. A small systematic bias was clear above water surfaces, e.g. the North sea, where Landsat-8's values were higher (approximately 0.01), relative to a typical surface reflectance of 0.03. Surface reflectance above vegetated terrain was also higher in most cases for Landsat-8. Differences of more than 0.2 were also observed. It is however important to note that these high differences could also be caused by the regridding process done in order to compare the two datasets.

Another aspect that became clear from the difference maps was that the Sentinel-2 dataset over the selected region consists of two 'tiles'. These tiles are the result of the way the Sentinel-2 Level-2 data is made available: it is delivered in 'granules' based on the UTM projection system. The focus area of this study is divided, almost precisely, in half in this tiling system of Sentinel-2. Since every tile is processed separately into the Level-2 dataset, the obvious discontinuity in the dataset can be explained.

The focus region comprises of different kinds of terrain which include: harbour/industrial, urban/populated, rural and (coastal) water bodies. These different terrain types were used to make a number of subsets, which were then used to make further comparisons between Landsat-8 and Sentinel-2. The first step was making 'relative difference' maps of these subsets. The different subsets were also used to create histograms and boxplots. These further supported the conclusions of a consistent offset above water surfaces and vegetation. On urban and industrial surfaces it also showed the variability which was visible in the difference maps.

In the following step the approach utilised was: the Sentinel-2 surface reflectance (SR) product and

the Landsat-8 SR product were regridded to the resolution of the TROPOMI observations (3.5 km x 7 km). On this grid the same difference maps were made. These still showed differences, but they were not as dominant as on the high resolution. The differences were close to zero, with extremes up to negative and positive 0.02. When compared to the differences between the currently used OMI LER albedo climatology on the TROPOMI grid and the Sentinel-2 SR dataset on this grid (which contained extreme differences well above 0.05), the differences between Sentinel-2 and Landsat-8 were much smaller. The first research question: *What is the accuracy of the Sentinel-2 surface reflectance product at its native resolution and on the spatial resolution of TROPOMI?* can therefore be answered in the following way: Sentinel-2's surface reflectance product is accurate when compared to Landsat-8's surface reflectance product, with a systematic bias of only 0.01 over water surfaces. Over land the range of differences was larger (exceeding 0.05), but these can largely be attributed to the different angles and the small offset of the pixel centres. When averaged and regridded onto the TROPOMI grid it can be considered even more accurate. This is due to the differences with Landsat-8 being greatly reduced since outliers on the resolution of the original data set are averaged out.

The next part of this research was using the different surface reflectance and albedo dataset in order to calculate *Air Mass Factors*. At the TROPOMI spatial resolution, and on its grid, the AMF values were calculated and their impact on the AMFs were determined by replacing the currently used surface albedo climatology with the surface reflectance derived from Sentinel-2. The AMFs were calculated by using altitude-resolved air mass factors which were computed by the DAK radiative transfer model and an assumed NO_2 vertical profile shape. Two vertical profile shapes were compared, with top heights of 400 and 800 metres respectively. In order to assess the uncertainty in the results, the same approach was followed by making use of the surface reflectance product of Landsat-8, instead of Sentinel-2.

Two periods in the spring of 2018 were analysed. These periods had excellent cloud free conditions and observations for the three satellites of interest: Sentinel-5p (TROPOMI), Sentinel-2 & Landsat-8. The first period was entirely on the 21st of April. The second period consisted of the 6th of May for TROPOMI & Sentinel-2 and the 7th of May for Landsat-8.

Based on Sentinel-2 surface reflectance data we find a spatially varying albedo-induced AMF-bias that ranges between -68.0% and 39.8% with a median bias of -10.4% for the 21st of April and values ranging from -48.6% to 37.0% with a median of -3.9% for 6th of May 2018. The results based on Landsat-8 are very similar, with AMF-biases which range between -53.9% and 36.3% with a median bias of -15.6% for the 21st of April and -43.4% to 33.5% with a median of -9.3% for 6th & 7th of May 2018. The remaining second-order differences can be attributed to the differences in the atmospheric correction schemes for the Sentinel-2 and Landsat-8 surface reflectance products, and differences in the viewing zenith angle and the solar zenith angle. These results show no strong dependence on the profile shape that was assumed ($0.03 < \Delta AMF < 0.07$).

The research question *What is the impact on the acurracy of the TROPOMI tropospheric NO_2 product of alternative prior surface reflectance information from Sentinel-2?* can therefore be answered by considering that the accuracy of the AMF values is improved by 10.4% on average when Sentinel-2's surface reflectance product is used instead of the OMI LER albedo climatology in April. Extreme improvements of up to 68.0% percent over water surfaces and vegetation have also been observed. Another important conclusion is the fact that over dark terrain, e.g. the North Sea, reduction of the AMF values can be seen which are caused by subtle changes in the surface reflectance values.

This exploratory study shows that the coarse spatial resolution of the OMI LER albedo climatology data base is one of the most critical limitations for a more accurate NO_2 product for (a region such as) the Greater Rotterdam region. The systematic bias in the S-5P tropospheric NO_2 product can be reduced if a better surface-albedo climatology is provided, i.e. at a spatial resolution that is preferably higher than the pixel size of the TROPOMI product. Further research is needed to determine which globally available dataset will be the optimal source for an improved surface albedo climatology. Depending on the location, the spatial resolution may be less critical (e.g. over terrain with small spatial gradients), whereas the effectiveness of the atmospheric correction scheme applied to the satellite sensor may be a more limiting factor.

A significant reduction of the systematic bias can only be guaranteed if the assumptions underlying the atmospheric correction scheme applied to the satellite sensor from which this surface albedo climatology is derived are consistent with the assumptions made in the cloud-aerosol model used for the S-5P NO_2-product. The latter aspect is not included in this study.

Certain effects were not or could not be investigated during this research. Therefore it is recommended for further research to look at a number of possible parameters and there influence. The first one being the seasonal dependence. Due to the limited number of available days in this research, being the end of April and the beginning of may, this seasonal influence has not been investigated in this research, while its effect may be significant. Another recommendation for future research would be to include different locations. Biases will be quite different depending on characteristics of landscape, e.g. dry/little vegetation compared to wet areas covered with vegetation. Furthermore it should be investigated if the Sentinel-2 surface reflectance product could be used to create a surface reflectance climatology at a resolution higher than the TROPOMI resolution (e.g. 2 km x 2 km), or if surface reflectance products from other sensors are more appropriate. It may be beneficial to create regional TROPOMI products (e.g. the Rijnmond) where the selection of a-priori datasets is optimised for local conditions.

Bibliography

[1] Spaceoffice News (2018).
With Tropomi, we are pushing things to the limit.
https://www.spaceoffice.nl/en/news/218/with-tropomi-we-are-pushing-things-to-the-limit.html

[2] Kleipool, Ludewig, Veefkind & Dobber (2013).
Level 1 lessons learned from OMI and TROPOMI.

[3] Esa, Sentinel Online (2018).
Sentinel-5 Heritage.
https://sentinel.esa.int/web/sentinel/missions/sentinel-5/overview/heritage

[4] Vlemmix (2011).
Tropospheric nitrogen dioxide inversions based on spectral measurements of scattered sunlight.

[5] ICPDR (2013).
Reducing nutrient pollution, challenges in agriculture.

[6] EPA (2016).
Basic Information about NO2.
https://www.epa.gov/no2-pollution/basic-information-about-no2#Effects

[7] Nagesh Kumar (2016).
Spatial and Spectral Resolutions.

[8] van Geffen, Eskes, Boersma, Maasakker & Veefkind (2018).
TROPOMI ATBD of the total and tropospheric NO_2 data products.
https://sentinel.esa.int/documents/247904/2476257/Sentinel-5P-TROPOMI-ATBD-NO2-data-products

[9] Platt & Stutz (2008).
Differential Optical Absorption Spectroscopy.

[10] Richter & Burrows (2013).
A multi wavelengths approach to the retrieval of Tropospheric NO2 from GOME measurements.

[11] Kleipool et al. (2008).
Earth surface reflectance climatology from 3 years of OMI data.

[12] Nayar, Ramamoorthi & Hanrahan (2009).
Basic Principles of Surface Reflectance.
https://www.cs.cmu.edu/afs/cs/academic/class/15462-f09/www/lec/lec8.pdf

[13] ESA (2014).
Introducing Sentinel-2.
http://www.esa.int/Our_Activities/Observing_the_Earth/Copernicus/Sentinel-2/Introducing_Sentinel-2

[14] Gunter's Space Page (2017).
Sentinel 2A, 2B, 2C, 2D.
https://space.skyrocket.de/doc_sdat/sentinel-2.htm

[15] Kaufman & Sendra (1988).
Algorithm for automatic atmospheric corrections to visible and near IR satellite imagery.

[16] Richter, Louis & Berthelot (2011).
Sentinel-2 MSI – Level 2A Products Algorithm Theoretical Basis Document.

[17] ESA.
Sentinel-2 - Level-2.

https://sentinel.esa.int/web/sentinel/user-guides/sentinel-2-msi/processing-levels/level-2

[18] USGS.
Landsat-8.

https://landsat.usgs.gov/landsat-8

[19] ESA, Sentinel-5P.
Level-2 Algorithms - NO2 Tropospheric, Stratospheric and Total Vertical Columns.

https://earth.esa.int/web/sentinel/technical-guides/sentinel-5p/level-2/no2-tropospheric-stratospheric-total-vertical-column

[20] USGS (2018).
Landsat-8 Product Guide.

[21] Levy, Remer, Tanré, Mattoo & Kaufman (2009).
Algorithm for Remote Sensing of tropospheric aerosol over dark targets from MODIS.

[22] NASA.
MODIS Aerosol Product.

https://modis.gsfc.nasa.gov/data/dataprod/mod04.php

[23] USGS (2016).
Landsat Surface Reflectance Level-2 Science Products.

https://landsat.usgs.gov/landsat-surface-reflectance-data-products

[24] Schaap et al. (2009).
Exploring the relation between aerosol optical depth and PM2.5 at Cabauw, the Netherlands.

[25] ESA, Sentinel-2.
Sentinel-2-msi product-types.

https://sentinel.esa.int/web/sentinel/user-guides/sentinel-2-msi/product-types

[26] ESA, (2017).
Sentinel-2 Products Specification Document.

https://sentinels.copernicus.eu/documents/247904/685211/Sentinel-2+Products+Specification+Document+%28PSD%29/0f7bedeb-9fbb-4b60-91aa-809162de456c

[27] ESA (2017).
TROPOMI.

https://www.esa.int/Our_Activities/Observing_the_Earth/Copernicus/Sentinel-5P/Tropomi

[28] Sportisse (2014).
Fundamentals in Air Pollution.

[29] Brohede (2002).
Differential Optical Absorption Spectroscopy - How does it work and what can it measure?

[30] De Haan, Bosma, Hovenier (1987).
The adding method for multiple scattering of polarized light

[31] Pinardi et al. (2018).
Validation of TROPOMI NO2 and HCHO vertical columns with UV-Vis DOAS and FTIR instruments

[32] McCamley (2014).
Characterising Vegetation Structure Using MODIS MultiAngular Data.